Nuclear Engineering and Design 64 (1981) 49–80
North-Holland Publishing Company

A SOLUTION PROCEDURE FOR THERMO-ELASTIC-PLASTIC AND CREEP PROBLEMS

Mark D. SNYDER and Klaus-Jürgen BATHE
Department of Mechanical Engineering, Massachusetts Institute of Technology, Cambridge, MA 02139, USA

Received 30 September 1980

An effective solution procedure for finite element thermo-elastic-plastic and creep analysis with temperature-dependent material properties is presented. The material model employed is summarized, the basic iterative equations are developed and the solution procedure is theoretically analyzed and numerically tested for its stability and accuracy properties.

1. Introduction

The application of the finite element method to the inelastic analysis of structures and continua has received considerable attention over the last fifteen years [1–21]. To a large extent, this effort has been motivated by the need to safety and economically predict material response under conditions of extreme mechanical and thermal loading. Some examples are the design and analysis of pressure vessels, ships, and aircraft, as well as the study of metal forming, welding, and nuclear weapon effects on soils and structures.

Based on extensive experience, the solution of problems with inelastic material behavior has proven to be much more difficult than the analysis of linear elastic behavior. The currently available solution procedures can be quite costly, unstable, and inaccurate. In addition, the models of inelastic material behavior in current engineering use are not always suitable for complex loading conditions. All of these factors have placed a severe constraint on the routine use of inelastic finite element analysis.

The cost of inelastic analysis is particularly high in three-dimensional calculations. However, a more critical factor is that considerable user knowledge and judgment are involved in selecting an appropriate solution strategy. In practice, this situation almost always means that obtaining a reliable solution requires some, if not extensive, numerical experimentation. There is surely a need for solution techniques with increased accuracy and stability properties as well as self-adaptive algorithms that adjust computational strategy as the solution proceeds.

Our objective in this paper is to present the development, analysis, and testing of a solution procedure for the finite element analysis of thermo-elastic-plastic and creep problems with temperature-dependent material properties. The solution procedure is based on a one-parameter integration method (the α-method) for a system of ordinary differential equations. This integration method, which contains the well-known Euler forward and backward methods, was previously proposed and analyzed for the finite element analysis of certain heat conduction [22,23] and viscoplasticity [3,4,6] problems. In this paper we use the α-method as the basis of an effective algorithm for the analysis of significantly more complex thermo-elastic-plastic and creep problems.

We first summarize in section 2 the formulation of the thermo-elastic-plastic and creep material model. Section 3 contains the development of the finite element solution procedure and a theoretical analysis of its stability charac teristics. The procedure has been implemented in the finite element computer program ADINA [21] and in section 4 we present and discuss the solutions for three test problems. The conclusions are contained in section 5.

* Invited paper, presented at the 5th International Conference on Structural Mechanics in Reactor Technology, Berlin (West), August 13–17, 1979.

All notation is defined in the text when it is first introduced. A left superscript denotes the time at which a quantity occurs. No left superscript indicates a finite increment. Differentiation with respect to time is indicated by an overhead dot. Right lower case subscripts denote the components of Cartesian vectors and tensors. Finally, right superscripts and subscripts contained within parentheses are iteration counters.

2. Thermo-elastic-plastic and creep material model

In this section we present a material model which includes the combined effects of thermoelasticity, thermoplasticity, and creep. All material properties (e.g., Young's modulus, yield stress, etc.) are allowed to vary with temperature. The thermoplasticity part of the model utilizes the von Mises yield function with the option of either isotropic or kinematic hardening. The creep formulation is a modified equation-of-state approach which is suitable for cyclic loading conditions.

2.1. Formulation of the model

A basic assumption in the formulation of the model is that the usual small strain tensor can be expressed as the sum of elastic, plastic, creep and thermal strains,

$$ {}^{\tau}e_{ij} = {}^{\tau}e_{ij}^{E} + {}^{\tau}e_{ij}^{P} + {}^{\tau}e_{ij}^{C} + {}^{\tau}e_{ij}^{TH} , \tag{1} $$

where

${}^{\tau}e_{ij}$ = component of total strain tensor,
${}^{\tau}e_{ij}^{E}$ = component of elastic strain tensor,
${}^{\tau}e_{ij}^{P}$ = component of plastic strain tensor,
${}^{\tau}e_{ij}^{C}$ = component of creep strain tensor,
${}^{\tau}e_{ij}^{TH}$ = component of thermal strain tensor,

This assumption allows the use of the so-called classical theories of plasticity and creep which make a distinction between time-dependent and time-independent inelastic strains.

The constitutive law for an isotropic, thermoelastic material with temperature-dependent moduli is [38,39],

$$ {}^{\tau}\sigma_{ij} = {}^{\tau}C_{ijrs}^{E}({}^{\tau}e_{rs} - {}^{\tau}e_{rs}^{P} - {}^{\tau}e_{rs}^{C} - {}^{\tau}e_{rs}^{TH}) , \tag{2} $$

where

${}^{\tau}C_{ijrs}^{E}$ = component of elastic constitutive tensor

$$ = {}^{\tau}\lambda\delta_{ij}\delta_{rs} + {}^{\tau}\mu(\delta_{ir}\delta_{js} + \delta_{is}\delta_{jr}) , $$

$$ {}^{\tau}\lambda = \frac{{}^{\tau}E\,{}^{\tau}\nu}{(1+{}^{\tau}\nu)(1-2\,{}^{\tau}\nu)} , $$

$$ {}^{\tau}\mu = \frac{{}^{\tau}E}{2(1+{}^{\tau}\nu)} , $$

${}^{\tau}E$ = Young's modulus,

${}^{\tau}\nu$ = Poisson's ratio,

δ_{ij} = Kronecker delta,

$$ {}^{\tau}e_{rs}^{TH} = {}^{\tau}\alpha_{m}({}^{\tau}\theta - \theta_{R})\,\delta_{rs} , $$

${}^{\tau}\theta$ = temperature,

${}^{\tau}\alpha_m$ = mean coefficient of thermal expansion,

θ_R = reference temperature.

The creep strain rate is determined using a modified equation-of-state approach which includes strain hardening for variable loading and the Oak Ridge National Laboratory auxiliary hardening rules for cyclic behavior [27,28]. The final result [18] is stated as

$$ {}^{\tau}\dot{e}_{ij}^{C} = {}^{\tau}\gamma\, {}^{\tau}s_{ij} , \tag{3} $$

where

${}^{\tau}s_{ij}$ = component of deviatoric stress tensor

$$ = {}^{\tau}\sigma_{ij} - \tfrac{1}{3}{}^{\tau}\sigma_{mm}\delta_{ij} , $$

$$ {}^{\tau}\gamma = \frac{3}{2}\frac{{}^{\tau}\dot{\bar{e}}^{C}}{{}^{\tau}\bar{\sigma}} , $$

${}^{\tau}\bar{\sigma}$ = von Mises effective stress

$$ = \sqrt{\tfrac{3}{2}\, {}^{\tau}s_{ij}\, {}^{\tau}s_{ij}} , $$

${}^{\tau}\dot{\bar{e}}^{C}$ = effective creep strain rate

$$ = f({}^{\tau}\sigma, {}^{\tau}\bar{e}^{H}, {}^{\tau}\theta) , $$

${}^{\tau}\bar{e}^{H}$ = modified effective creep strain.

The plastic strain rate is calculated using the classical theory of time-independent plasticity [29–39]. The general form of the yield or loading function for non-isothermal conditions is assumed to be

$$ {}^{\tau}F = {}^{\tau}F({}^{\tau}\sigma_{ij}, {}^{\tau}\alpha_{ij}, {}^{\tau}\sigma_y) , \tag{4} $$

where ${}^{\tau}\alpha_{ij}$ and ${}^{\tau}\sigma_y$ depend on the history of plastic deformation and temperature. For elastic behavior, ${}^{\tau}F < 0$, and for plastic behavior, ${}^{\tau}F = 0$.

As a consequence of Drucker's postulate for stable inelastic materials under isothermal conditions, the yield function ${}^{\tau}F$ defines a convex yield surface in nine-dimensional stress space. Furthermore, when stress and plastic strain rate axes are coincident the plastic strain rate vector is normal to the yield surface. In developing a noniso-thermal plasticity model, it is assumed that ${}^{\tau}F$ defines a convex yield surface in a ten-dimensional stress–temperature space and that the isothermal normality condition remains valid [31]. Thus, the plastic strain rate is defined by

$$ {}^{\tau}\dot{e}_{ij}^{P} = {}^{\tau}\Lambda \frac{\partial\, {}^{\tau}F}{\partial\, {}^{\tau}\sigma_{ij}} , \tag{5} $$

where ${}^{\tau}\Lambda$ = positive scalar variable.

The calculation of ${}^{\tau}\Lambda$ requires that a hardening rule be selected. A hardening rule describes the change in the yield surface with continuing plastic deformation. Two commonly used hardening rules are isotropic hardening [39], and kinematic hardening [33].

2.1.1. Isotropic hardening rule

The isotropic hardening rule for isothermal conditions assumes that the size of the yield surface increases uniformly while its center remains fixed in nine-dimensional stress space. The size of the yield surface, as defined by

the yield stress, is based on either the plastic work or the accumulated effective plastic strain. In the following extension of the isotropic hardening rule to non-isothermal conditions [31,37], it is assumed that the yield stress depends on the accumulated effective plastic strain and instantaneous temperature.

The von Mises yield function for non-isothermal, isotropic hardening can be written as

$$ {}^{\tau}F = \tfrac{1}{2}\,{}^{\tau}s_{lm}\,{}^{\tau}s_{lm} - \tfrac{1}{3}\,{}^{\tau}\sigma_y^2 , \tag{6} $$

where

$ {}^{\tau}\sigma_y $ = yield stress

$ = {}^{\tau}\sigma_y({}^{\tau}\bar{e}^{\mathrm{P}}, {}^{\tau}\theta) $,

$ {}^{\tau}\bar{e}^{\mathrm{P}} $ = accumulated effective plastic strain

$ = \int_0^{\tau} {}^{\tau}\dot{\bar{e}}^{\mathrm{P}}\,\mathrm{d}t $,

$ {}^{\tau}\dot{\bar{e}}^{\mathrm{P}} $ = effective plastic strain rate

$ = \sqrt{\tfrac{2}{3}\,{}^{\tau}\dot{e}^{\mathrm{P}}_{ij}\,{}^{\tau}\dot{e}^{\mathrm{P}}_{ij}} $.

The objective is to determine ${}^{\tau}\Lambda$ in terms of the current strain and temperature rates. Taking the derivative of eq. (2) with respect to time and then substituting from eq. (5) results in

$$ {}^{\tau}\dot{\sigma}_{ij} = {}^{\tau}C^{\mathrm{E}}_{ijmn}\left({}^{\tau}\dot{e}_{mn} - {}^{\tau}\Lambda\frac{\partial\,{}^{\tau}F}{\partial\,{}^{\tau}\sigma_{mn}} - {}^{\tau}\dot{e}^{\mathrm{C}}_{mn} - {}^{\tau}\dot{e}^{\mathrm{TH}}_{mn}\right) + {}^{\tau}\dot{C}^{\mathrm{E}}_{ijcd}\,{}^{\tau}e^{\mathrm{E}}_{cd} . \tag{7} $$

During plastic straining, the stress–temperature state remains on the yield surface so that

$$ {}^{\tau}\dot{F} = \frac{\partial\,{}^{\tau}F}{\partial\,{}^{\tau}\sigma_{ij}}\,{}^{\tau}\dot{\sigma}_{ij} + \frac{\partial\,{}^{\tau}F}{\partial\,{}^{\tau}\alpha_{ij}}\,{}^{\tau}\dot{\alpha}_{ij} + \frac{\partial\,{}^{\tau}F}{\partial\,{}^{\tau}\sigma_y}\,{}^{\tau}\dot{\sigma}_y = 0 . \tag{8} $$

Considering eq. (6), it can readily be shown that

$$ \frac{\partial\,{}^{\tau}F}{\partial\,{}^{\tau}\alpha_{ij}} = 0 , \tag{9} $$

$$ \frac{\partial\,{}^{\tau}F}{\partial\,{}^{\tau}\sigma_y} = -\tfrac{2}{3}\,{}^{\tau}\sigma_y , \tag{10} $$

$$ \frac{\partial\,{}^{\tau}F}{\partial\,{}^{\tau}\sigma_{ij}} = {}^{\tau}s_{ij} , \tag{11} $$

$$ {}^{\tau}\dot{\sigma}_y = \frac{\partial\,{}^{\tau}\sigma_y}{\partial\,{}^{\tau}\bar{e}^{\mathrm{P}}}\,{}^{\tau}\dot{\bar{e}}^{\mathrm{P}} + \frac{\partial\,{}^{\tau}\sigma_y}{\partial\,{}^{\tau}\theta}\,{}^{\tau}\dot{\theta} . \tag{12} $$

Substituting eqs. (9)–(12) into eq. (8) and using the previously stated definitions of ${}^{\tau}\dot{\bar{e}}^{\mathrm{P}}$ and ${}^{\tau}\dot{e}^{\mathrm{P}}_{ij}$ results in

$$ {}^{\tau}s_{ij}\,{}^{\tau}\dot{\sigma}_{ij} = \tfrac{2}{3}\,{}^{\tau}\sigma_y\left[\frac{\partial\,{}^{\tau}\sigma_y}{\partial\,{}^{\tau}\bar{e}^{\mathrm{P}}}\,{}^{\tau}\Lambda\sqrt{\tfrac{2}{3}\,{}^{\tau}s_{ij}\,{}^{\tau}s_{ij}} + \frac{\partial\,{}^{\tau}\sigma_y}{\partial\,{}^{\tau}\theta}\,{}^{\tau}\dot{\theta}\right]. \tag{13} $$

Since ${}^{\tau}F = 0$ during plastic straining,

$$ {}^{\tau}s_{ij}\,{}^{\tau}s_{ij} = \tfrac{2}{3}\,{}^{\tau}\sigma_y^2 , \tag{14} $$

and hence eq. (13) simplifies to

$$ {}^{\tau}s_{ij}\,{}^{\tau}\dot{\sigma}_{ij} = \tfrac{2}{3}\,{}^{\tau}\sigma_y\left[\tfrac{2}{3}\,{}^{\tau}\sigma_y\,{}^{\tau}\Lambda\frac{\partial\,{}^{\tau}\sigma_y}{\partial\,{}^{\tau}\bar{e}^{\mathrm{P}}} + \frac{\partial\,{}^{\tau}\sigma_y}{\partial\,{}^{\tau}\theta}\,{}^{\tau}\dot{\theta}\right]. \tag{15} $$

Premultiplying eq. (7) by ${}^{\tau}s_{ij}$, setting the result equal to eq. (15) and solving for ${}^{\tau}\Lambda$ gives

$$ {}^{\tau}\Lambda = \frac{{}^{\tau}s_{ij}\,{}^{\tau}C^{\mathrm{E}}_{ijmn}({}^{\tau}\dot{e}_{mn} - {}^{\tau}\dot{e}^{\mathrm{C}}_{mn} - {}^{\tau}\dot{e}^{\mathrm{TH}}_{mn}) + {}^{\tau}s_{ij}\,{}^{\tau}\dot{C}^{\mathrm{E}}_{ijcd}\,{}^{\tau}e^{\mathrm{E}}_{cd} - \frac{2}{3}\,{}^{\tau}\sigma_y \dfrac{\partial\,{}^{\tau}\sigma_y}{\partial\,{}^{\tau}\theta}\,{}^{\tau}\dot{\theta}}{\frac{4}{9}\,{}^{\tau}\sigma_y^2 \dfrac{\partial\,{}^{\tau}\sigma_y}{\partial\,{}^{\tau}\bar{e}^{\mathrm{P}}} + {}^{\tau}s_{ij}\,{}^{\tau}C^{\mathrm{E}}_{ijmn}\,{}^{\tau}s_{mn}} . \tag{16} $$

In order to further evaluate the above expression for ${}^{\tau}\Lambda$, it is necessary to obtain $\partial\,{}^{\tau}\sigma_y/\partial\,{}^{\tau}e^{\mathrm{P}}$ and $\partial\,{}^{\tau}\sigma_y/\partial\,{}^{\tau}\theta$. It is assumed that a relationship between ${}^{\tau}\sigma_y$, ${}^{\tau}\bar{e}^{\mathrm{P}}$, and ${}^{\tau}\theta$ can be derived from the data obtained in a series of tensile tests at different temperatures using virgin material specimens. This data is used to develop the idealized, bilinear, engineering stress-strain curves shown in fig. 1.

To convert the curves shown in fig. 1 to stress–plastic strain curves, we have for constant temperature ${}^{\tau}\theta$ and ${}^{\tau}\sigma \geqslant {}^{\tau}\sigma_{yv}$,

$$ {}^{\tau}\sigma = {}^{\tau}\sigma_{yv} + {}^{\tau}E_{\mathrm{T}}\left({}^{\tau}e - \frac{{}^{\tau}\sigma_{yv}}{{}^{\tau}E}\right), \tag{17} $$

$$ {}^{\tau}e^{\mathrm{P}} = {}^{\tau}e - {}^{\tau}\sigma/{}^{\tau}E , \tag{18} $$

Combining the above equations and noting that the current stress is the current yield stress (i.e., ${}^{\tau}\sigma = {}^{\tau}\sigma_y$) results in

$$ {}^{\tau}\sigma_y = \frac{{}^{\tau}E\,{}^{\tau}E_{\mathrm{T}}}{{}^{\tau}E - {}^{\tau}E_{\mathrm{T}}}\,{}^{\tau}e^{\mathrm{P}} + {}^{\tau}\sigma_{yv} . \tag{19} $$

Thus, eq. (19) gives the relationship between yield stress and plastic strain for monotonic uniaxial loading at constant temperature. The curves described by eq. (19) are shown in fig. 2.

It is now assumed that eq. (19) relates the yield stress and the accumulated effective plastic strain for multiaxial loading conditions. Additionally, it is assumed that the relation holds regardless of the history leading to ${}^{\tau}\bar{e}^{\mathrm{P}}$.

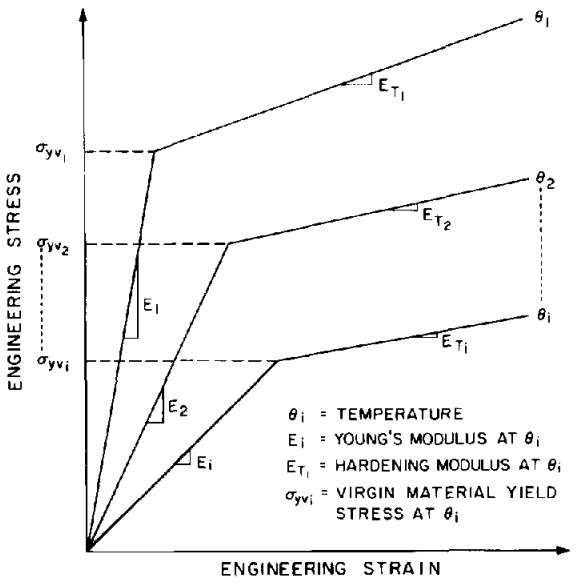

Fig. 1. Idealized engineering stress–strain curves.

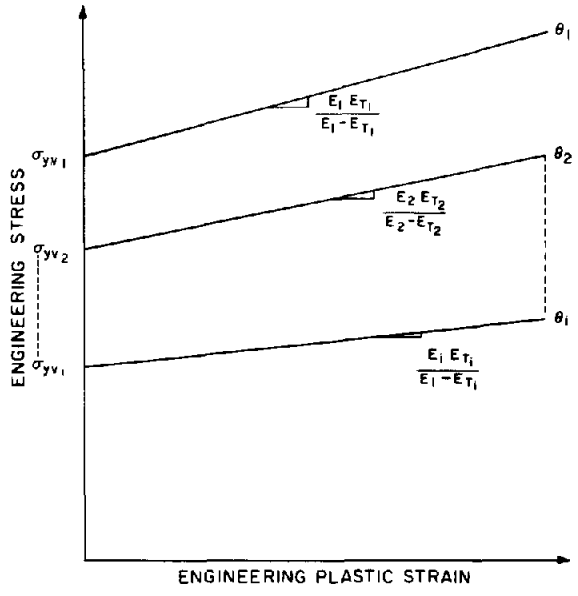

Fig. 2. Idealized engineering stress–plastic strain curves.

We then obtain

$$\frac{\partial\, {}^{\tau}\sigma_y}{\partial\, {}^{\tau}\bar{e}^{\mathrm{P}}} = \frac{{}^{\tau}E\, {}^{\tau}E_{\mathrm{T}}}{{}^{\tau}E - {}^{\tau}E_{\mathrm{T}}} \tag{20}$$

and

$$\frac{\partial\, {}^{\tau}\sigma_y}{\partial\, {}^{\tau}\theta} = {}^{\tau}\bar{e}^{\mathrm{P}}\, \frac{\partial}{\partial\, {}^{\tau}\theta}\left(\frac{{}^{\tau}E\, {}^{\tau}E_{\mathrm{T}}}{{}^{\tau}E - {}^{\tau}E_{\mathrm{T}}}\right) + \frac{\partial\, {}^{\tau}\sigma_{yv}}{\partial\, {}^{\tau}\theta}. \tag{21}$$

Substituting eqs. (20) and (21) into eq. (16) and using the definitions of ${}^{\tau}\sigma_y$, ${}^{\tau}C^{\mathrm{E}}_{ijrs}$ and ${}^{\tau}s_{ij}$ yields:

$${}^{\tau}\Lambda = \frac{{}^{\tau}\mu\, {}^{\tau}s_{mn}({}^{\tau}e_{mn} - {}^{\tau}\dot{e}^{\mathrm{C}}_{mn} - {}^{\tau}\dot{e}^{\mathrm{TH}}_{mn}) + {}^{\tau}\dot{\mu}\, {}^{\tau}s_{cd}\, {}^{\tau}e^{\mathrm{E}}_{cd} - \frac{{}^{\tau}\sigma_y}{3}\left[{}^{\tau}\bar{e}^{\mathrm{P}}\, \frac{\partial}{\partial\, {}^{\tau}\theta}\left(\frac{{}^{\tau}E\, {}^{\tau}E_{\mathrm{T}}}{{}^{\tau}E - {}^{\tau}E_{\mathrm{T}}}\right) + \frac{\partial\, {}^{\tau}\sigma_{yv}}{\partial\, {}^{\tau}\theta}\, {}^{\tau}\dot{\theta}\right]}{\frac{2\, {}^{\tau}\sigma_y^2}{3}\left[{}^{\tau}\mu + \frac{1}{3}\frac{{}^{\tau}E\, {}^{\tau}E_{\mathrm{T}}}{{}^{\tau}E - {}^{\tau}E_{\mathrm{T}}}\right]} \tag{22}$$

2.1.2. Kinematic hardening rule

The kinematic hardening rule for isothermal conditions assumes that the size of the yield surface remains constant and that the yield surface can translate as a rigid body in nine-dimensional stress space. The translation is a measure of the hardening of the material and the incremental translation components are generally assumed to be linearly related to the incremental plastic strains.

In the extension of the rule to non-isothermal conditions [31,36,37], it is assumed that both the size of the yield surface and the hardening of the material can depend on temperature. The von Mises yield function for non-isothermal, kinematic hardening can be written as

$${}^{\tau}F = \tfrac{1}{2}({}^{\tau}s_{lm} - {}^{\tau}\alpha_{lm})({}^{\tau}s_{lm} - {}^{\tau}\alpha_{lm}) - \tfrac{1}{3}{}^{\tau}\sigma_y^2\,, \tag{23}$$

where

${}^{\tau}\sigma_y$ = yield stress

$= {}^{\tau}\sigma_y({}^{\tau}\theta)$,

${}^{\tau}\alpha_{lm}$ = component of yield surface translation tensor

$$= \int_0^{\tau} {}^{t}\dot{\alpha}_{lm}\, \mathrm{d}t\,,$$

${}^{\tau}\dot{\alpha}_{lm} = {}^{\tau}C\, {}^{\tau}\dot{e}^{\mathrm{I}}_{lm}$,

${}^{\tau}C$ = hardening parameter

$= {}^{\tau}C({}^{\tau}\theta)$.

Following the development of eq. (22), it can be shown [18] that

$${}^{\tau}\Lambda = \frac{({}^{\tau}s_{ij} - {}^{\tau}\alpha_{ij})\, {}^{\tau}C^{\mathrm{E}}_{ijmn}({}^{\tau}\dot{e}_{mn} - {}^{\tau}\dot{e}^{\mathrm{C}}_{mn} - {}^{\tau}\dot{e}^{\mathrm{TH}}_{mn}) + ({}^{\tau}s_{ij} - {}^{\tau}\alpha_{ij})\, {}^{\tau}\dot{C}^{\mathrm{E}}_{ijcd}\, {}^{\tau}e^{\mathrm{E}}_{cd} - \frac{2}{3}\, {}^{\tau}\sigma_y\, \frac{\partial\, {}^{\tau}\sigma_y}{\partial\, {}^{\tau}\theta}\, {}^{\tau}\dot{\theta}}{\frac{2}{3}{}^{\tau}\sigma_y^2\, {}^{\tau}C + ({}^{\tau}s_{ij} - {}^{\tau}\alpha_{ij})\, {}^{\tau}C^{\mathrm{E}}_{ijmn}({}^{\tau}s_{mn} - {}^{\tau}\alpha_{mn})} \tag{29}$$

To further evaluate eq. (24), it is necessary to obtain both ${}^{\tau}C$ and $\partial\, {}^{\tau}\sigma_y/\partial\, {}^{\tau}\theta$. As was done for the case of isotropic hardening, we use the idealized, bilinear, engineering stress–strain curves shown in fig. 1 and now assume that the

relationship between ${}^{\tau}\sigma_y$ and ${}^{\tau}\theta$ is the same as that between the virgin material yield stress and temperature. That is, ${}^{\tau}\sigma_y$ is simply the virgin material yield stress corresponding to ${}^{\tau}\theta$.

For the hardening parameter ${}^{\tau}C$, consider a case of uniaxial loading at constant temperature such that

$$
\begin{aligned}
&{}^{\tau}\sigma_{11} \neq 0 , \qquad \text{all other } {}^{\tau}\sigma_{ij} = 0 ,\\
&{}^{\tau}\dot{\sigma}_{11} \neq 0 , \qquad \text{all other } {}^{\tau}\dot{\sigma}_{ij} = 0 ,\\
&{}^{\tau}s_{22} = {}^{\tau}s_{33} = -\tfrac{1}{2}\,{}^{\tau}s_{11} ,\\
&{}^{\tau}e^{\mathrm{P}}_{22} = {}^{\tau}e^{\mathrm{P}}_{33} = -\tfrac{1}{2}\,{}^{\tau}e^{\mathrm{P}}_{11} , \qquad \text{all other } {}^{\tau}e^{\mathrm{P}}_{ij} = 0 ,\\
&{}^{\tau}\dot{e}^{\mathrm{P}}_{22} = {}^{\tau}\dot{e}^{\mathrm{P}}_{33} = -\tfrac{1}{2}\,{}^{\tau}\dot{e}^{\mathrm{P}}_{11} , \qquad \text{all other } {}^{\tau}\dot{e}^{\mathrm{P}}_{ij} = 0 ,\\
&{}^{\tau}\sigma_y = \text{constant} .
\end{aligned}
\tag{25}
$$

Evaluating ${}^{\tau}F = 0$ and ${}^{\tau}\dot{F} = 0$ for the above loading condition results in

$$
({}^{\tau}s_{11} - {}^{\tau}\alpha_{11})^2 = \tfrac{2}{3}\,{}^{\tau}\sigma_y^2 \tag{26}
$$

and

$$
({}^{\tau}s_{11} - {}^{\tau}\alpha_{11})({}^{\tau}\dot{\sigma}_{11} - \tfrac{3}{2}\,{}^{\tau}C\,{}^{\tau}\dot{e}^{\mathrm{P}}_{11}) = 0 . \tag{27}
$$

The above equations require that

$$
{}^{\tau}\dot{\sigma}_{11} = \tfrac{3}{2}\,{}^{\tau}C\,{}^{\tau}\dot{e}^{\mathrm{P}}_{11} , \tag{28}
$$

or

$$
\mathrm{d}\sigma_{11} = \tfrac{3}{2}\,{}^{\tau}C\,\mathrm{d}e^{\mathrm{P}}_{11} . \tag{29}
$$

Referring to the idealized stress–plastic strain curves shown in fig. 2, the infinitesimal stress increment $\mathrm{d}\sigma$ at constant temperature is given by

$$
\mathrm{d}\sigma = \frac{{}^{\tau}E\,{}^{\tau}E_{\mathrm{T}}}{{}^{\tau}E - {}^{\tau}E_{\mathrm{T}}}\,\mathrm{d}e^{\mathrm{P}} . \tag{30}
$$

Comparing eqs. (29) and (30) shows that

$$
{}^{\tau}C = \frac{2}{3}\,\frac{{}^{\tau}E\,{}^{\tau}E_{\mathrm{T}}}{{}^{\tau}E - {}^{\tau}E_{\mathrm{T}}} . \tag{31}
$$

Substituting eq. (31) into eq. (24) and using the definitions of ${}^{\tau}\sigma_y$, ${}^{\tau}C^{\mathrm{E}}_{ijrs}$, and ${}^{\tau}s_{ij}$, we obtain

$$
{}^{\tau}\Lambda = \frac{{}^{\tau}\mu({}^{\tau}s_{mn} - {}^{\tau}\alpha_{mn})({}^{\tau}\dot{e}_{mn} - {}^{\tau}\dot{e}^{\mathrm{C}}_{mn} - {}^{\tau}\dot{e}^{\mathrm{TH}}_{mn}) + {}^{\tau}\dot{\mu}({}^{\tau}s_{mn} - {}^{\tau}\alpha_{mn})\,{}^{\tau}e^{\mathrm{E}}_{mn} - \dfrac{{}^{\tau}\sigma_{yv}}{3}\,\dfrac{\partial\,{}^{\tau}\sigma_{yv}}{\partial\,{}^{\tau}\theta}\,{}^{\tau}\dot{\theta}}{\dfrac{2\,{}^{\tau}\sigma_y^2}{3}\left[{}^{\tau}\mu + \dfrac{1}{3}\,\dfrac{{}^{\tau}E\,{}^{\tau}E_{\mathrm{T}}}{{}^{\tau}E - {}^{\tau}E_{\mathrm{T}}}\right]} . \tag{32}
$$

2.2. *Applicability of the model*

The model is suitable for use in small strain and displacement analysis. However, it is also directly applicable to problems involving small strains and large rotations [20].

When using the model for practical engineering analyses, it is important to be aware of the limitations of the theories upon which it is based. The classical theory of time-independent plasticity does not accurately predict

material behavior under general, non-radial loading conditions [27–29]. In addition, the O.R.N.L. auxiliary strain hardening rules were developed for radial or near-radial loading. Based on limited experimental results [27,28], the kinematic hardening formulation is recommended for cyclic, radial or near-radial loading. The isotropic hardening formulation is recommended only for situations involving monotonically increasing, radial or near-radial loading.

3. Solution procedure

The proposed solution procedure is based on a one-parameter integration method for ordinary differential equations (the α-method) which is used in conjunction with the thermo-elastic-plastic and creep material model developed in section 2. For a range of values of the parameter, this integration method has been shown to be unconditionally stable for certain heat conduction [22,23] and viscoplasticity problems [3,4,6].

The solution procedure uses one time step size for the calculation of nodal point displacements and a smaller one for element integration point stresses, plastic strains, and creep strains. This approach is based on the observation that for many problems of engineering interest involving inelastic behavior, the time-wise variation in the stresses and inelastic strains is greater than that of the displacements [16–19].

In the following, we investigate the stability of the solution procedure via the calculations for the element integration point stresses. We assume that the stability characteristics associated with these particular calculations carry over to the other solution variables. Only the case of isotropic hardening is examined. However, similar conclusions can be reached for kinematic hardening [20].

3.1. The α-method

Consider a system of first-order, ordinary differential equations of the form

$$ {}^{\tau}\dot{\boldsymbol{x}} = {}^{\tau}\boldsymbol{A}\ {}^{\tau}\boldsymbol{x} , \tag{33} $$

where τ denotes some arbitrary time. Assuming that an approximate numerical solution ${}^{t}\boldsymbol{x}$ is known, the next approximate solution ${}^{t+\Delta t}\boldsymbol{x}$ is given by

$$ {}^{t+\Delta t}\boldsymbol{x} = {}^{t}\boldsymbol{x} + {}^{t+\alpha\Delta t}\dot{\boldsymbol{x}}\,\Delta t , \tag{34} $$

where

$$ {}^{t+\alpha\Delta t}\dot{\boldsymbol{x}} = {}^{t+\alpha\Delta t}\boldsymbol{A}\ {}^{t+\alpha\Delta t}\boldsymbol{x} , \tag{35} $$

$$ {}^{t+\alpha\Delta t}\boldsymbol{x} = (1-\alpha)\,{}^{t}\boldsymbol{x} + \alpha\,{}^{t+\Delta t}\boldsymbol{x} , \quad 0 \leqslant \alpha \leqslant 1 , \tag{36} $$

$$ {}^{t+\alpha\Delta t}\boldsymbol{A} = {}^{t+\alpha\Delta t}\boldsymbol{A}({}^{t+\alpha\Delta t}\boldsymbol{x},\ t+\alpha\Delta t) . \tag{37} $$

Substituting eqs. (35)–(37) into eq. (34) yields:

$$ [\boldsymbol{I} - \alpha\Delta t\ {}^{t+\alpha\Delta t}\boldsymbol{A}]\ {}^{t+\Delta t}\boldsymbol{x} = [\boldsymbol{I} + (1-\alpha)\,\Delta t\ {}^{t+\alpha\Delta t}\boldsymbol{A}]\ {}^{t}\boldsymbol{x} . \tag{38} $$

Eq. (38) must generally be solved for ${}^{t+\Delta t}\boldsymbol{x}$ in an iterative manner, but a direct solution is possible when ${}^{\tau}\boldsymbol{A}$ is a constant matrix. Note that $\alpha = 0$ and $\alpha = 1$ are the Euler forward and backward methods, respectively. Additionally, $\alpha = \frac{1}{2}$ corresponds to the usual trapezoidal rule only when ${}^{\tau}\boldsymbol{A}$ is a constant matrix. It can be shown [20] that $\alpha = 0, 1$ have local truncation errors of $O(\Delta t^2)$ and that $\alpha = \frac{1}{2}$ has a local truncation error of $O(\Delta t^3)$.

3.2. Theoretical stability analysis

In investigating the solution procedure's stability characteristics, we are primarily interested in how roundoff errors are propagated through the numerical computations. For stability, it is required that roundoff errors not

be magnified as the numerical calculations progress. We note that the following analysis is not concerned with the truncation errors of the solution method. Such errors exist even if all arithmetic operations are performed exactly. While the truncation error directly affects the accuracy of a numerical method, stability is a primary requirement for an accurate solution. On the other hand, a stable solution can still be inaccurate due to large truncation errors or an excessive number of solution steps which result in roundoff accumulation (but not stepwise magnification).

In the development of the solution procedure in section 3.3, it will be shown that the calculations for the element integration point stresses lead to nonlinear algebraic equations of the form

$$[I - \alpha\Delta\tau\, {}^{\tau+\Delta\tau}A\, {}^{\tau+\Delta\tau}C]\, {}^{\tau+\Delta\tau}x = [I + (1-\alpha)\,\Delta\tau\, {}^{\tau+\Delta\tau}A\, {}^{\tau+\alpha\Delta\tau}C + {}^{\tau+\Delta\tau}AS]\, {}^{\tau}x + L + {}^{\tau+\Delta\tau}AT\,, \tag{39}$$

where

${}^{\tau}x$ = known vector of stresses,
${}^{\tau+\Delta\tau}x$ = unknown vector of stresses,
L, T = known vectors with time-dependent components
${}^{\tau+\Delta\tau}A, S$ = known square matrices with time-dependent components
${}^{\tau+\alpha\Delta\tau}C$ = square matrix which is a function of the known and unknown solution variables
I = identity matrix.

Additionally, we require that ${}^{\tau+\Delta\tau}A$ be negative definite and that ${}^{\tau+\Delta\tau}C$ be positive semi-definite.

Now assume that there is some roundoff error ${}^{\tau}\epsilon$ in the numerical solution at time τ such that

$${}^{\tau}x^* = {}^{\tau}x + {}^{\tau}\epsilon\,. \tag{40}$$

If all arithmetic calculations are performed exactly, then the solution at time $\tau + \Delta\tau$ is

$$[I - \alpha\Delta\tau\, {}^{\tau+\Delta\tau}A\, {}^{\tau+\alpha\Delta\tau}C^*]\, {}^{\tau+\Delta\tau}x^* = [I + (1-\alpha)\,\Delta\tau\, {}^{\tau+\Delta\tau}A\, {}^{\tau+\alpha\Delta\tau}C^* + {}^{\tau+\Delta\tau}AS]\, {}^{\tau}x^* + L + {}^{\tau+\Delta\tau}AT\,, \tag{41}$$

where

$${}^{\tau+\Delta\tau}x^* = {}^{\tau+\Delta\tau}x + {}^{\tau+\Delta\tau}\epsilon \tag{42}$$

and ${}^{\tau+\Delta\tau}\epsilon$ = propagated roundoff error and ${}^{\tau+\alpha\Delta\tau}C^*$ = perturbed version of ${}^{\tau+\alpha\Delta\tau}C$ due to ${}^{\tau}\epsilon$ and ${}^{\tau+\Delta\tau}\epsilon$.

It can be seen by referring to the definitions of ${}^{\tau+\alpha\Delta\tau}C$ in sections 3.3 and 3.4 that ${}^{\tau+\alpha\Delta\tau}C^*$ is also a positive semi-definite matrix.

Now consider the generalized eigenproblem [40]:

$${}^{\tau+\alpha\Delta\tau}C^*\phi^* = \lambda\, {}^{\tau+\Delta\tau}A^{-1}\phi^*\,, \tag{43}$$

with solutions

$${}^{\tau+\alpha\Delta\tau}C^*\Phi^* = {}^{\tau+\Delta\tau}A^{-1}\Phi^*\Lambda^*\,, \tag{44}$$

$$\Phi^* = [\phi_1^*, \ldots, \phi_n^*]\,,$$

$$\Lambda^* = \mathrm{diag}[\lambda_i^*], \quad \lambda_i^* \leqslant 0\,.$$

The orthogonality properties of the eigenvectors are such that

$$\Phi^{*\mathrm{T}}\, {}^{\tau+\Delta\tau}A^{-1}\Phi^* = I\,, \tag{45}$$

$$\Phi^{*\mathrm{T}}\, {}^{\tau+\alpha\Delta\tau}C^*\Phi^* = \Lambda^*\,. \tag{46}$$

The n eigenvectors span an n-dimensional vector space. Therefore, we can write

$${}^{\tau+\Delta\tau}x = \Phi^*\, {}^{\tau+\Delta\tau}z \tag{47}$$

$${}^{\tau}x = \Phi^*\, {}^{\tau}z\,, \tag{48}$$

$$^{\tau+\Delta\tau}\boldsymbol{\varepsilon} = \boldsymbol{\Phi}^{*\,\tau+\Delta\tau}\boldsymbol{e}\,, \tag{49}$$

$$^{\tau}\boldsymbol{\varepsilon} = \boldsymbol{\Phi}^{*\,\tau}\boldsymbol{e}\,. \tag{50}$$

Premultiplying eq. (41) by $^{\tau+\Delta\tau}\boldsymbol{A}^{-1}$ yields:

$$[^{\tau+\Delta\tau}\boldsymbol{A}^{-1} - \alpha\Delta\tau\,^{\tau+\alpha\Delta\tau}\boldsymbol{C}^{*}]\;^{\tau+\Delta\tau}\boldsymbol{x}^{*} = [^{\tau+\Delta\tau}\boldsymbol{A}^{-1} + (1-\alpha)\,\Delta\tau\,^{\tau+\alpha\Delta\tau}\boldsymbol{C}^{*} + \boldsymbol{S}]\;^{\tau}\boldsymbol{x}^{*} + {}^{\tau+\Delta\tau}\boldsymbol{A}^{-1}\boldsymbol{L} + \boldsymbol{T}\,. \tag{51}$$

Substituting eqs. (47)–(50) into eq. (51), premultiplying by $\boldsymbol{\Phi}^{*}$ and using the orthogonality properties, eqs. (45) and (46), results in

$$[\boldsymbol{I} - \alpha\Delta\tau\,\boldsymbol{\Lambda}^{*}]\;(^{\tau+\Delta\tau}\boldsymbol{z} + {}^{\tau+\Delta\tau}\boldsymbol{e}) = [\boldsymbol{I} + (1-\alpha)\,\Delta\tau\,\boldsymbol{\Lambda}^{*}]\;(^{\tau}\boldsymbol{z} + {}^{\tau}\boldsymbol{e}) + \boldsymbol{\Phi}^{*\mathrm{T}}\,\boldsymbol{S}\boldsymbol{\Phi}^{*}(^{\tau}\boldsymbol{z} + {}^{\tau}\boldsymbol{e}) + \boldsymbol{\Phi}^{*\mathrm{T}}\,{}^{\tau+\Delta\tau}\boldsymbol{A}^{-1}\boldsymbol{L} + \boldsymbol{\Phi}^{*\mathrm{T}}\,\boldsymbol{T}\,. \tag{52}$$

To obtain an expression relating $^{\tau}\boldsymbol{e}$ and $^{\tau+\Delta\tau}\boldsymbol{e}$, we assume that $^{\tau+\alpha\Delta\tau}\boldsymbol{C}^{*} \simeq {}^{\tau+\alpha\Delta\tau}\boldsymbol{C}$, $\boldsymbol{\Phi}^{*} \simeq \boldsymbol{\Phi}$, and $\boldsymbol{\Lambda}^{*} \simeq \boldsymbol{\Lambda}$. The error terms now separate directly out of eq. (52) and we have

$$[\boldsymbol{I} - \alpha\Delta\tau\boldsymbol{\Lambda}]\;{}^{\tau+\Delta\tau}\boldsymbol{e} = [\boldsymbol{I} + (1-\alpha)\,\Delta\tau\boldsymbol{\Lambda}]\;{}^{\tau}\boldsymbol{e} + \boldsymbol{\Phi}^{\mathrm{T}}\,\boldsymbol{S}\boldsymbol{\Phi}\,{}^{\tau}\boldsymbol{e}\,. \tag{53}$$

For the jth component of $^{\tau+\Delta\tau}\boldsymbol{e}$, we obtain

$${}^{\tau+\Delta\tau}e_j = \frac{1 + (1-\alpha)\,\Delta\tau\lambda_j}{1 - \alpha\Delta\tau\lambda_j}\,{}^{\tau}e_j + \frac{\{\boldsymbol{\Phi}^{\mathrm{T}}\,\boldsymbol{S}\,\boldsymbol{\Phi}\,{}^{\tau}\boldsymbol{e}\}_j}{1 - \alpha\Delta\tau\lambda_j}\,. \tag{54}$$

Note that the second term on the right-hand side couples $^{\tau+\Delta\tau}e_j$ to all the components of $^{\tau}\boldsymbol{e}$.

As discussed previously, stability means that any roundoff error present at time τ is not magnified when the solution for time $\tau + \Delta\tau$ is calculated. Specifically, we require that

$$|{}^{\tau+\Delta\tau}\boldsymbol{\epsilon}^{\mathrm{T}}\,{}^{\tau+\Delta\tau}\boldsymbol{A}^{-1}\;{}^{\tau+\Delta\tau}\boldsymbol{\epsilon}| \leqslant |{}^{\tau}\boldsymbol{\varepsilon}^{\mathrm{T}}\,{}^{\tau+\Delta\tau}\boldsymbol{A}^{-1}\,{}^{\tau}\boldsymbol{\varepsilon}|\,. \tag{55}$$

Substituting eqs. (49) and (50) into eq. (55) and using eq. (45) results in

$$|{}^{\tau+\Delta\tau}\boldsymbol{e}^{\mathrm{T}}\,{}^{\tau+\Delta\tau}\boldsymbol{e}| \leqslant |{}^{\tau}\boldsymbol{e}^{\mathrm{T}}\,{}^{\tau}\boldsymbol{e}|\,. \tag{56}$$

A sufficient, but not necessary condition for eq. (56) to hold is

$$|{}^{\tau+\Delta\tau}e_j| \leqslant |{}^{\tau}e_j|\,. \tag{57}$$

Consider eq. (54) and examine the cases of $\boldsymbol{S} \equiv \boldsymbol{0}$ and $\boldsymbol{S} \neq \boldsymbol{0}$. In the first case, eq. (57) is satisfied if

$$\left|\frac{1 + (1-\alpha)\Delta\tau\lambda_j}{1 - \alpha\Delta\tau\lambda_j}\right| \leqslant 1\,. \tag{58}$$

Recalling that $\lambda_j \leqslant 0$, $0 \leqslant \alpha \leqslant 1$, and $\Delta\tau > 0$, some algebraic manipulation shows that eq. (58) is satisfied for all $\Delta\tau > 0$ when $\alpha \geqslant \frac{1}{2}$. Thus, the algorithm can be made unconditionally stable. On the other hand, if $\alpha < \frac{1}{2}$ then eq. (58) requires

$$\Delta\tau \leqslant \frac{1}{(2\alpha - 1)\,\lambda_j}\,. \tag{59}$$

We note that this conditional stability limit may not be useful for practical computations since λ_j generally depends on the unknown solution at time $\tau + \Delta\tau$. The only exception is when $\alpha = 0$, in which case λ_j is determined by the known conditions at time τ.

However, when $\boldsymbol{S} \neq \boldsymbol{0}$ there is no a priori information available concerning the second term on the right-hand side of eq. (54). At present, the best approach is to make all of the coefficients of $^{\tau}e_i$ as small as possible. This means having the condition in eq. (58) as well as requiring that the denominator of the above-mentioned term be as large as possible. For specified $\Delta\tau$ and $\lambda_j \leqslant 0$, this latter condition occurs when $\alpha = 1$.

3.3. Special case

In this section we develop an algorithm for the special case in which a common time step size is used for all solution variables. Assuming that a numerical solution has been obtained at discrete time points Δt, $2\Delta t$, ..., t, the solution for $t + \Delta t$ is desired.

3.3.1. Equilibrium and constitutive equations

At time $t + \Delta t$, consider the virtual work equation for an isoparametric, finite element assemblage [40] and the constitutive equations for a thermo-elastic-plastic and creep material with isotropic hardening. All equations are expressed in vector form [18] as

$$\sum_{m=1}^{N} \int_{v^{(m)}} B_L^{\mathrm{T}}\, {}^{t+\Delta t}\boldsymbol{\sigma}\, \mathrm{d}v = {}^{t+\Delta t}R\,, \tag{60}$$

$${}^{t+\Delta t}\boldsymbol{\sigma} = {}^{t+\Delta t}C^{\mathrm{E}}\,({}^{t+\Delta t}e - {}^{t+\Delta t}e^{\mathrm{P}} - {}^{t+\Delta t}e^{\mathrm{C}} - {}^{t+\Delta t}e^{\mathrm{TH}})\,, \tag{61}$$

$${}^{\tau}\dot{e}^{\mathrm{P}} = {}^{\tau}\Lambda D\, {}^{\tau}\boldsymbol{\sigma}\,, \tag{62}$$

$${}^{\tau}\dot{e}^{\mathrm{C}} = {}^{\tau}\gamma D\, {}^{\tau}\boldsymbol{\sigma}\,, \tag{63}$$

$${}^{t+\Delta t}e^{\mathrm{TH}} = {}^{t+\Delta t}\alpha_m({}^{t+\Delta t}\theta - \theta_{\mathrm{R}})\,\boldsymbol{\delta}\,, \tag{64}$$

where

$${}^{t+\Delta t}e = B_L\, {}^{t+\Delta t}U \tag{65}$$

and

B_L = total strain-displacement transformation matrix,
${}^{t+\Delta t}U$ = nodal point displacement vector,
${}^{t+\Delta t}R$ = nodal point external load vector,
N = number of elements in the assemblage,
D = deviatoric stress operator matrix,
$\boldsymbol{\delta}^{\mathrm{T}}$ = [1,1,1,0,0,0].

Henceforth, the summation sign in eq. (60) will be dropped for convenience, but the summation is implied for all subsequent volume integrals. Although eqs. (61)–(64) are valid at any point in the structure or continuum, only the stresses and strains at the element integration points [40] will be of interest.

Substituting eqs. (61) and (65) into eq. (60) results in

$${}^{t+\Delta t}K^{\mathrm{E}}\, {}^{t+\Delta t}U = {}^{t+\Delta t}R + \int_{v} B_L^{\mathrm{T}}\, {}^{t+\Delta t}C^{\mathrm{E}}({}^{t+\Delta t}e^{\mathrm{P}} + {}^{t+\Delta t}e^{\mathrm{C}} + {}^{t+\Delta t}e^{\mathrm{TH}})\, \mathrm{d}v\,, \tag{66}$$

where

$${}^{t+\Delta t}K^{\mathrm{E}} = \int_{v} B_L^{\mathrm{T}}\, {}^{t+\Delta t}C^{\mathrm{E}} B_L\, \mathrm{d}v \tag{67}$$

is the elastic stiffness matrix.

3.3.2. Algorithm development

The α-method is used to obtain ${}^{t+\Delta t}\boldsymbol{e}^{\mathrm{P}}$ and ${}^{t+\Delta t}\boldsymbol{e}^{\mathrm{C}}$. Quantities at time $t + \Delta t$ are first decomposed as

$$ {}^{t+\Delta t}\boldsymbol{e}^{\mathrm{P}} = {}^{t}\boldsymbol{e}^{\mathrm{P}} + \boldsymbol{e}^{\mathrm{P}} , \tag{68} $$

$$ {}^{t+\Delta t}\boldsymbol{e}^{\mathrm{C}} = {}^{t}\boldsymbol{e}^{\mathrm{C}} + \boldsymbol{e}^{\mathrm{C}} \tag{69} $$

and then the increments are given by

$$ \boldsymbol{e}^{\mathrm{P}} = \Delta t\, {}^{t+\alpha\Delta t}\dot{\boldsymbol{e}}^{\mathrm{P}} = \Delta t\, {}^{t+\alpha\Delta t}\Lambda \boldsymbol{D}\, {}^{t+\alpha\Delta t}\boldsymbol{\sigma} , \tag{70} $$

$$ \boldsymbol{e}^{\mathrm{C}} = \Delta t\, {}^{t+\alpha\Delta t}\dot{\boldsymbol{e}}^{\mathrm{C}} = \Delta t\, {}^{t+\alpha\Delta t}\gamma \boldsymbol{D}\, {}^{t+\alpha\Delta t}\boldsymbol{\sigma} , \tag{71} $$

where

$$ {}^{t+\alpha\Delta t}\boldsymbol{\sigma} = (1 - \alpha)\, {}^{t}\boldsymbol{\sigma} + \alpha\, {}^{t+\Delta t}\boldsymbol{\sigma} \tag{72} $$

and

$$ \begin{aligned} {}^{t+\alpha\Delta t}\Lambda &= {}^{t+\alpha\Delta t}\Lambda\,({}^{t+\alpha\Delta t}\boldsymbol{\sigma},\ {}^{t+\alpha\Delta t}\dot{\boldsymbol{e}},\ {}^{t+\alpha\Delta t}\dot{\boldsymbol{e}}^{\mathrm{C}},\ {}^{t+\alpha\Delta t}\dot{\theta},\ \ldots) , \\ {}^{t+\alpha\Delta t}\gamma &= {}^{t+\alpha\Delta t}\gamma\,({}^{t+\alpha\Delta t}\boldsymbol{\sigma},\ {}^{t+\alpha\Delta t}\bar{e}^{\mathrm{H}},\ {}^{t+\alpha\Delta t}\theta) . \end{aligned} \tag{73} $$

Eqs. (61), (64), (66), and (68) to (73) are a coupled set of nonlinear algebraic equations where eqs. (61), (64) and (68) to (73) apply at each integration point.

Nonlinear algebraic equations generally require an iterative solution procedure [42]. Starting with the simplest approach – successive substitution – an appropriate algorithm is

$$ {}^{t+\Delta t}\boldsymbol{e}^{\mathrm{C}(i+1)} = {}^{t}\boldsymbol{e}^{\mathrm{C}} + \Delta t\, {}^{t+\alpha\Delta t}\gamma^{(i)} \boldsymbol{D}\, {}^{t+\alpha\Delta t}\boldsymbol{\sigma}^{(i)} , \tag{74} $$

$$ {}^{t+\Delta t}\boldsymbol{e}^{\mathrm{P}(i+1)} = {}^{t}\boldsymbol{e}^{\mathrm{P}} + \Delta t\, {}^{t+\alpha\Delta t}\Lambda^{(i)} \boldsymbol{D}\, {}^{t+\alpha\Delta t}\boldsymbol{\sigma}^{(i)} , \tag{75} $$

$$ {}^{t+\Delta t}\boldsymbol{K}^{\mathrm{E}}\, {}^{t+\Delta t}\boldsymbol{U}^{(i+1)} = {}^{t+\Delta t}\boldsymbol{R} + \int_{v} \boldsymbol{B}_L^{\mathrm{T}}\, {}^{t+\Delta t}\boldsymbol{C}^{\mathrm{E}} ({}^{t+\Delta t}\boldsymbol{e}^{\mathrm{P}(i+1)} + {}^{t+\Delta t}\boldsymbol{e}^{\mathrm{C}(i+1)} + {}^{t+\Delta t}\boldsymbol{e}^{\mathrm{TH}})\, \mathrm{d}v , \tag{76} $$

$$ {}^{t+\Delta t}\boldsymbol{\sigma}^{(i+1)} = {}^{t+\Delta t}\boldsymbol{C}^{\mathrm{E}} ({}^{t+\Delta t}\boldsymbol{e}^{(i+1)} - {}^{t+\Delta t}\boldsymbol{e}^{\mathrm{P}(i+1)} - {}^{t+\Delta t}\boldsymbol{e}^{\mathrm{C}(i+1)} - {}^{t+\Delta t}\boldsymbol{e}^{\mathrm{TH}}) , \qquad i = 0, 1, 2, \ldots . \tag{77} $$

The right superscript i is the iteration number and $i = 0$ refers to conditions at time t.

The above scheme can be rewritten by defining

$$ \Delta \boldsymbol{U}^{(i+1)} = {}^{t+\Delta t}\boldsymbol{U}^{(i+1)} - {}^{t+\Delta t}\boldsymbol{U}^{(i)} . \tag{78} $$

Substituting eq. (78) into eq. (76) and using eqs. (65) and (67) results in

$$ {}^{t+\Delta t}\boldsymbol{K}^{\mathrm{E}} \Delta \boldsymbol{U}^{(i+1)} = {}^{t+\Delta t}\boldsymbol{R} - \int_{v} \boldsymbol{B}_L^{\mathrm{T}}\, {}^{t+\Delta t}\boldsymbol{C}^{\mathrm{E}} ({}^{t+\Delta t}\boldsymbol{e}^{(i)} - {}^{t+\Delta t}\boldsymbol{e}^{\mathrm{P}(i+1)} - {}^{t+\Delta t}\boldsymbol{e}^{\mathrm{C}(i+1)} - {}^{t+\Delta t}\boldsymbol{e}^{\mathrm{TH}})\, \mathrm{d}v . \tag{79} $$

Noting the similarity between the right-hand sides of eqs. (77) and (79), the successive substitution algorithm is now written as

$$ {}^{t+\Delta t}\boldsymbol{e}^{\mathrm{C}(i+1)} = {}^{t}\boldsymbol{e}^{\mathrm{C}} + \Delta t\, {}^{t+\alpha\Delta t}\gamma^{(i)}\, \boldsymbol{D}\, {}^{t+\alpha\Delta t}\boldsymbol{\sigma}^{(i)} , \tag{80} $$

$$ {}^{t+\Delta t}\boldsymbol{e}^{\mathrm{P}(i+1)} = {}^{t}\boldsymbol{e}^{\mathrm{P}} + \Delta t\, {}^{t+\alpha\Delta t}\Lambda^{(i)}\, \boldsymbol{D}\, {}^{t+\alpha\Delta t}\boldsymbol{\sigma}^{(i)} , \tag{81} $$

$$ {}^{t+\Delta t}\boldsymbol{\sigma}^{(i+1)} = {}^{t+\Delta t}\boldsymbol{C}^{\mathrm{E}} ({}^{t+\Delta t}\boldsymbol{e}^{(i)} - {}^{t+\Delta t}\boldsymbol{e}^{\mathrm{P}(i+1)} - {}^{t+\Delta t}\boldsymbol{e}^{\mathrm{C}(i+1)} - {}^{t+\Delta t}\boldsymbol{e}^{\mathrm{TH}}) , \tag{82} $$

$$ {}^{t+\Delta t}\boldsymbol{K}^{\mathrm{E}} \Delta \boldsymbol{U}^{(i+1)} = {}^{t+\Delta t}\boldsymbol{R} - \int_{v} \boldsymbol{B}_L^{\mathrm{T}}\, {}^{t+\Delta t}\boldsymbol{\sigma}^{(i+1)}\, \mathrm{d}v , \tag{83} $$

$$^{t+\Delta t}U^{(i+1)} = {}^{t+\Delta t}U^{(i)} + \Delta U^{(i+1)}\,, \qquad i = 0, 1, 2, \ldots\,. \tag{84}$$

Assuming that the iteration converges, $\Delta U^{(i+1)} \to \mathbf{0}$ and hence all of the governing equations are satisfied. Furthermore, by iterating with $\Delta U^{(i+1)}$ instead of $^{t+\Delta t}U^{(i+1)}$, it is possible to use stiffness matrices other than $^{t+\Delta t}K^{\mathrm{E}}$ in eq. (83) so as to obtain faster convergence [24].

The scheme described in eqs. (81)–(84) has two immediate drawbacks. Successive substitution can have a slow rate-of-convergence [42]. Additionally, disk I/O operations are required in each iteration (assuming that integration point variables are not continually stored in-core). If the restriction of no disk writing during the iteration is imposed, then the following algorithm (still based on successive substitution) can be used.

displacement loop — integration point loop

$$^{t+\Delta t}e^{\mathrm{C}(i)}_{(k+1)} = {}^{t}e^{\mathrm{C}} + \Delta t\,{}^{t+\alpha\Delta t}\gamma^{(i)}_{(k)} D\,{}^{t+\alpha\Delta t}\boldsymbol{\sigma}^{(i)}_{(k)}\,, \tag{85}$$

$$^{t+\Delta t}e^{\mathrm{P}(i)}_{(k+1)} = {}^{t}e^{\mathrm{P}} + \Delta t\,{}^{t+\alpha\Delta t}\Lambda^{(i)}_{(k)} D\,{}^{t+\alpha\Delta t}\boldsymbol{\sigma}^{(i)}_{(k)}\,, \tag{86}$$

$$^{t+\Delta t}\boldsymbol{\sigma}^{(i)}_{(k+1)} = {}^{t+\Delta t}C^{\mathrm{E}}\left({}^{t+\Delta t}e^{(i)} - {}^{t+\Delta t}e^{\mathrm{P}(i)}_{(k+1)} - {}^{t+\Delta t}e^{\mathrm{C}(i)}_{(k+1)} - {}^{t+\Delta t}e^{\mathrm{TH}}\right), \qquad k = 0, 1, 2, \ldots\,, \tag{87}$$

$$^{t+\Delta t}K^{\mathrm{E}}\Delta U^{(i+1)} = {}^{t+\Delta t}R - \int_{v} B_L^{\mathrm{T}}\,{}^{t+\Delta t}\boldsymbol{\sigma}^{(i)}\,\mathrm{d}v\,, \tag{88}$$

$$^{t+\Delta t}U^{(i+1)} = {}^{t+\Delta t}U^{(i)} + \Delta U^{(i+1)}\,, \qquad i = 0, 1, 2, \ldots\,. \tag{89}$$

The right subscript k is the integration point loop iteration counter and the right superscript i is the displacement loop iteration counter. Note that $k = 0$ indicates conditions at time t and that $^{t+\Delta t}U^{(0)} = {}^{t}U$, $^{t+\Delta t}e^{(0)} = {}^{t}e$.

The integration point loop iteration continues until a steady value is obtained for $^{t+\Delta t}\boldsymbol{\sigma}^{(i)}$. The displacement loop iteration continues until $\Delta U^{(i+1)} \to \mathbf{0}$. When i = 0, the integration point calculations are performed only once (i.e., for $k = 0$ only).

The above algorithm trades disk writing operations for more computational effort. For each value of $^{t+\Delta t}e^{(i)}$, it is necessary to calculate $^{t+\Delta t}\boldsymbol{\sigma}^{(i)}$, $^{t+\Delta t}e^{\mathrm{P}(i)}$, and $^{t+\Delta t}e^{\mathrm{C}(i)}$ by starting from the corresponding values at time t. On the other hand, the converged integration point loop values satisfy the constitutive equations (within the approximations of the α-method). This can be advantageous in plasticity problems when yielding or unloading occurs during a solution step [24].

However, both computational loops can still suffer from slow rates-of-convergence. Considering first the integration point loop, one possible improvement is to solve eqs. (85)–(87) using Newton–Raphson iteration [42]. In three dimensional analysis, this means that a system of eighteen algebraic equations must be repeatedly solved at each integration point. The increased rate-of-convergence could easily be offset by the increase in computational effort.

As a compromise, the following scheme is proposed. It assumes that the stress-dependent terms in the creep constitutive law are the most troublesome from a convergence point-of-view. From eqs. (69) and (71), define

$$^{t+\alpha\Delta t}f = {}^{t}e^{\mathrm{C}} + e^{\mathrm{C}} = {}^{t}e^{\mathrm{C}} + \Delta t\,{}^{t+\alpha\Delta t}\gamma\, D\,{}^{t+\alpha\Delta t}\boldsymbol{\sigma}\,. \tag{90}$$

Expanding $^{t+\alpha\Delta t}f$ in a two-term Taylor series [42] about the kth approximate solution $^{t+\alpha\Delta t}\boldsymbol{\sigma}_{(k)}$ yields:

$$^{t+\alpha\Delta t}f_{(k+1)} = {}^{t+\alpha\Delta t}f_{(k)} + \left[\frac{\partial\,{}^{t+\alpha\Delta t}f}{\partial\,{}^{t+\alpha\Delta t}\boldsymbol{\sigma}}\right]_{(k)} \left({}^{t+\alpha\Delta t}\boldsymbol{\sigma}_{(k+1)} - {}^{t+\alpha\Delta t}\boldsymbol{\sigma}_{(k)}\right), \tag{91}$$

where the Jacobian matrix is

$$\left[\frac{\partial\,{}^{t+\alpha\Delta t}f}{\partial\,{}^{t+\alpha\Delta t}\boldsymbol{\sigma}}\right]_{(k)} = \Delta t\left[D\,{}^{t+\alpha\Delta t}\boldsymbol{\sigma}\,\frac{\partial\,{}^{t+\alpha\Delta t}\gamma}{\partial\,{}^{t+\alpha\Delta t}\boldsymbol{\sigma}} + {}^{t+\alpha\Delta t}\gamma\, D\right]_{(k)}. \tag{92}$$

The evaluation of the term $\partial\, {}^{t+\alpha\Delta t}\gamma / \partial\, {}^{t+\alpha\Delta t}\boldsymbol{\sigma}$ depends on the particular type of creep law being considered [20]. Substituting eqs. (88)–(90) into eq. (61) and solving for ${}^{t+\Delta t}\boldsymbol{\sigma}_{(k+1)}$ results in;

$$\left[\boldsymbol{I} + \alpha\Delta t\, {}^{t+\Delta t}\boldsymbol{C}^{\mathrm{E}}\left[\boldsymbol{D}\, {}^{t+\alpha\Delta t}\boldsymbol{\sigma}\frac{\partial\, {}^{t+\alpha\Delta t}\gamma}{\partial\, {}^{t+\alpha\Delta t}\boldsymbol{\sigma}} + {}^{t+\Delta t}\gamma\, \boldsymbol{D}\right]_{(k)}\right] {}^{t+\Delta t}\boldsymbol{\sigma}_{(k+1)} =$$

$$\begin{aligned}
&{}^{t+\Delta t}\boldsymbol{C}^{\mathrm{E}}(\boldsymbol{B}_L\, {}^{t+\Delta t}\boldsymbol{U} - {}^{t+\Delta t}\boldsymbol{e}^{\mathrm{P}} - {}^{t}\boldsymbol{e}^{\mathrm{C}} - {}^{t+\Delta t}\boldsymbol{e}^{\mathrm{TH}} - \Delta t\, {}^{t+\alpha\Delta t}\gamma_{(k)}\, \boldsymbol{D}\, {}^{t+\alpha\Delta t}\boldsymbol{\sigma}_{(k)}) \\
&+ \alpha\Delta t\, {}^{t+\Delta t}\boldsymbol{C}^{\mathrm{E}}\left[\boldsymbol{D}\, {}^{t+\alpha\Delta t}\boldsymbol{\sigma}\frac{\partial\, {}^{t+\alpha\Delta t}\gamma}{\partial\, {}^{t+\alpha\Delta t}\boldsymbol{\sigma}} + {}^{t+\alpha\Delta t}\gamma\, \boldsymbol{D}\right]_{(k)} {}^{t+\Delta t}\boldsymbol{\sigma}_{(k)} .
\end{aligned} \tag{93}$$

When $i > 0$, eqs. (85)–(87) (the integration point loop) are replaced by

$${}^{t+\Delta t}\boldsymbol{e}^{\mathrm{P}(i)}_{(k+1)} = {}^{t}\boldsymbol{e}^{\mathrm{P}} + \Delta t\, {}^{t+\alpha\Delta t}\Lambda^{(i)}_{(k)}\, \boldsymbol{D}\, {}^{t+\alpha\Delta t}\boldsymbol{\sigma}^{(i)}_{(k)} , \tag{94}$$

$$\left[\boldsymbol{I} + \alpha\Delta t\, {}^{t+\Delta t}\boldsymbol{C}^{\mathrm{E}}\left[\boldsymbol{D}\, {}^{t+\alpha\Delta t}\boldsymbol{\sigma}^{(i)}\frac{\partial\, {}^{t+\alpha\Delta t}\gamma^{(i)}}{\partial\, {}^{t+\alpha\Delta t}\boldsymbol{\sigma}^{(i)}} + {}^{t+\alpha\Delta t}\gamma^{(i)}\boldsymbol{D}\right]_{(k)}\right] {}^{t+\Delta t}\boldsymbol{\sigma}^{(i)}_{(k+1)} =$$

$$\begin{aligned}
&{}^{t+\Delta t}\boldsymbol{C}^{\mathrm{E}}({}^{t+\Delta t}\boldsymbol{e}^{(i)} - {}^{t+\Delta t}\boldsymbol{e}^{\mathrm{P}(i)}_{(k+1)} - {}^{t}\boldsymbol{e}^{\mathrm{C}} - {}^{t+\Delta t}\boldsymbol{e}^{\mathrm{TH}} - \Delta t\, {}^{t+\alpha\Delta t}\gamma^{(i)}_{(k)}\boldsymbol{D}\, {}^{t+\alpha\Delta t}\boldsymbol{\sigma}^{(i)}_{(k)}) \\
&+ \alpha\Delta t\, {}^{t+\Delta t}\boldsymbol{C}^{\mathrm{E}}\left[\boldsymbol{D}\, {}^{t+\alpha\Delta t}\boldsymbol{\sigma}^{(i)}\frac{\partial\, {}^{t+\alpha\Delta t}\gamma^{(i)}}{\partial\, {}^{t+\alpha\Delta t}\boldsymbol{\sigma}^{(i)}} + {}^{t+\alpha\Delta t}\gamma^{(i)}\boldsymbol{D}\right]_{(k)} {}^{t+\Delta t}\boldsymbol{\sigma}^{(i)}_{(k)} ,
\end{aligned} \tag{95}$$

$$\begin{aligned}
{}^{t+\Delta t}\boldsymbol{e}^{\mathrm{C}(i)}_{(k+1)} &= {}^{t}\boldsymbol{e}^{\mathrm{C}} + \Delta t\, {}^{t+\alpha\Delta t}\gamma^{(i)}_{(k)}\, \boldsymbol{D}\, {}^{t+\alpha\Delta t}\boldsymbol{\sigma}^{(i)}_{(k)} \\
&+ \alpha\Delta t\left[\boldsymbol{D}\, {}^{t+\alpha\Delta t}\boldsymbol{\sigma}^{(i)}\frac{\partial\, {}^{t+\alpha\Delta t}\gamma^{(i)}}{\partial\, {}^{t+\alpha\Delta t}\boldsymbol{\sigma}^{(i)}} + {}^{t+\alpha\Delta t}\gamma^{(i)}\boldsymbol{D}\right]_{(k)} ({}^{t+\Delta t}\boldsymbol{\sigma}^{(i)}_{(k+1)} - {}^{t+\alpha\Delta t}\boldsymbol{\sigma}^{(i)}_{(k)}) .
\end{aligned} \tag{96}$$

However, when $i = 0$ we still use eqs. (85)–(87) and the integration point calculations are performed only once (i.e., for $k = 0$ only). We also note that when there are no creep effects, the above algorithm degenerates back to successive substitution.

In the displacement loop, the rate-of-convergence can be improved by several methods. The most common approach is to use an elastic-plastic [2,17], elastic-creep [10] or elastic-plastic-creep [14,15] stiffness matrix in eq. (88). Alternatively, the use of matrix updating and search algorithms has been found to be highly effective [24].

3.3.3. Stability analysis

To investigate the stability of the solution procedure we establish a set of equations relating ${}^{t+\Delta t}\boldsymbol{\sigma}$ and ${}^{t}\boldsymbol{\sigma}$ at each integration point in the finite element assemblage. First, the decompositions

$$\begin{aligned}
&{}^{t+\Delta t}\boldsymbol{U} = {}^{t}\boldsymbol{U} + \boldsymbol{U} , \qquad {}^{t+\Delta t}\boldsymbol{C}^{\mathrm{E}} = {}^{t}\boldsymbol{C}^{\mathrm{E}} + \boldsymbol{C}^{\mathrm{E}} , \\
&{}^{t+\Delta t}\boldsymbol{e}^{\mathrm{TH}} = {}^{t}\boldsymbol{e}^{\mathrm{TH}} + \boldsymbol{e}^{\mathrm{TH}} , \qquad {}^{t+\Delta t}\boldsymbol{R} = {}^{t}\boldsymbol{R} + \boldsymbol{R} ,
\end{aligned} \tag{97}$$

are substituted into eqs. (61) and (66) along with eqs. (65) and (67)–(69) so as to obtain

$${}^{t+\Delta t}\boldsymbol{\sigma} = {}^{t+\Delta t}\boldsymbol{C}^{\mathrm{E}}(\boldsymbol{B}_L\boldsymbol{U} - \boldsymbol{e}^{\mathrm{P}} - \boldsymbol{e}^{\mathrm{C}} - \boldsymbol{e}^{\mathrm{TH}}) + (\boldsymbol{I} + \boldsymbol{C}^{\mathrm{E}}\, {}^{t}\boldsymbol{F}^{\mathrm{E}})\, {}^{t}\boldsymbol{\sigma} \tag{98}$$

and

$${}^{t+\Delta t}\boldsymbol{K}^{\mathrm{E}}\boldsymbol{U} = {}^{t}\boldsymbol{R} + \boldsymbol{R} + \int_{v}\boldsymbol{B}_L^{\mathrm{T}}\, {}^{t+\Delta t}\boldsymbol{C}^{\mathrm{E}}(\boldsymbol{e}^{\mathrm{P}} + \boldsymbol{e}^{\mathrm{C}} + \boldsymbol{e}^{\mathrm{TH}})\, \mathrm{d}v - \int_{v}\boldsymbol{B}_L^{\mathrm{T}}(\boldsymbol{I} + \boldsymbol{C}^{\mathrm{E}}\, {}^{t}\boldsymbol{F}^{\mathrm{E}})\, {}^{t}\boldsymbol{\sigma}\, \mathrm{d}v , \tag{99}$$

where

$$ {}^{t}F^{E}\,{}^{t}\sigma = {}^{t}e - {}^{t}e^{P} - {}^{t}e^{C} - {}^{t}e^{TH} . \tag{100} $$

Assuming an equilibrium configuration at time t, the corresponding virtual work equation is

$$ \int_{v} B_L^{T}\,{}^{t}\sigma \, dv = {}^{t}R \tag{101} $$

and hence eq. (97) simplies to

$$ {}^{t+\Delta t}K^{E}U = R + \int_{v} B_L^{T}\,{}^{t+\Delta t}C^{E}(e^{P} + e^{C} + e^{TH})\, dv - \int_{v} B_L^{T} C^{E}\,{}^{t}F^{E}\,{}^{t}\sigma \, dv . \tag{102} $$

In isoparametric finite element analysis, the volume integrals in eq. (102) are typically evaluated using Gauss numerical integration [40]. That is, a volume integral over the element assemblage can be expressed as

$$ \int_{v} f(x)\, dv = \sum_{i=1}^{N} \int_{v^{(i)}} f(x)\, dv = \sum_{j=1}^{M} w_j f(x_j) , \tag{103} $$

where

w_j = Gauss weighting factor; $w_j > 0$,
N = number of elements,
M = number of integration points,

Following the approach taken in [5], we define super matrices and vectors where each submatrix and subvector corresponds to a particular integration point (denoted by a right subscript).

$$ \tilde{B}_L = \begin{bmatrix} B_{L_1} \\ (6 \times n) \\ \hline B_{L_2} \\ \vdots \\ B_{L_M} \\ (6M \times n) \end{bmatrix} , \tag{104} $$

$$ {}^{t}\tilde{\Sigma} = \begin{bmatrix} {}^{t}\sigma_1 \\ (6 \times 1) \\ \hline {}^{t}\sigma_2 \\ \vdots \\ {}^{t}\sigma_M \\ (6M \times 1) \end{bmatrix} , \tag{105} $$

$$ {}^{t+\Delta t}C^{E} = \begin{bmatrix} {}^{t+\Delta t}C_1^{E} & & \\ (6 \times 6) & & \\ & {}^{t+\Delta t}C_2^{E} & \\ & & \ddots \\ & (6M \times 6M) & {}^{t+\Delta t}C_M^{E} \end{bmatrix} , \tag{106} $$

$$\tilde{D} = \begin{bmatrix} D & & \\ & \ddots & \\ & & D \end{bmatrix}, \quad \begin{matrix} (6 \times 6) \\ (6M \times 6M) \end{matrix} \tag{107}$$

$$\tilde{W} = \begin{bmatrix} w_1 I & & \\ & \ddots & \\ & & w_M I \end{bmatrix}, \quad \begin{matrix} (6 \times 6) \\ (6M \times 6M) \end{matrix} \tag{108}$$

where n is the number of degrees-of-freedom in the element assemblage. In addition, the super matrices $\tilde{C}^{\mathrm{E}}$, ${}^{t}\tilde{F}^{\mathrm{E}}$, and $\tilde{F}^{\mathrm{E}}$ are defined to be of the same form as ${}^{t+\Delta t}\tilde{C}^{\mathrm{E}}$, the super vectors. ${}^{t+\Delta t}\tilde{\Sigma}$ and $\tilde{E}^{\mathrm{TH}}$ are of the same form as ${}^{t}\tilde{\Sigma}$, and the super matrices ${}^{t+\alpha\Delta t}\tilde{\gamma}$ and ${}^{t+\alpha\Delta t}\tilde{\Lambda}$ are of the same form as $\tilde{W}$. Using eqs. (103)–(108), the volume integrals in eq. (102) are expressed as

$$\int_v B_L^{\mathrm{T}}\, {}^{t+\Delta t}C^{\mathrm{E}}(e^{\mathrm{P}} + e^{\mathrm{C}} + e^{\mathrm{TH}})\, \mathrm{d}v = \tilde{B}_L^{\mathrm{T}}\, {}^{t+\Delta t}\tilde{C}^{\mathrm{E}}\tilde{W}(\tilde{E}^{\mathrm{P}} + \tilde{E}^{\mathrm{TH}}), \tag{109}$$

$$\int_v B_L^{\mathrm{T}} C^{\mathrm{E}}\, {}^{t}F^{\mathrm{E}}\, {}^{t}\sigma\, \mathrm{d}v = \tilde{B}_L^{\mathrm{T}}\, \tilde{C}^{\mathrm{E}}\, {}^{t}\tilde{F}^{\mathrm{E}}\tilde{W}\, {}^{t}\tilde{\Sigma}. \tag{110}$$

Substituting eq. (72) into eqs. (70) and (71) results in

$$e^{\mathrm{P}} = \Delta t\, {}^{t+\alpha\Delta t}\Lambda\, D[(1-\alpha)\, {}^{t}\sigma + {}^{t+\Delta t}\sigma], \tag{111}$$

$$e^{\mathrm{C}} = \Delta t\, {}^{t+\alpha\Delta t}\gamma\, D[(1-\alpha)\, {}^{t}\sigma + \alpha\, {}^{t+\Delta t}\sigma] \tag{112}$$

and hence the corresponding super vectors are

$$\tilde{E}^{\mathrm{P}} = \Delta t\, {}^{t+\alpha\Delta t}\Lambda\tilde{D}[(1-\alpha)\, {}^{t}\tilde{\Sigma} + \alpha\, {}^{t+\Delta t}\tilde{\Sigma}], \tag{113}$$

$$\tilde{E}^{\mathrm{C}} = \Delta t\, {}^{t+\alpha\Delta t}\tilde{\gamma}\tilde{D}[(1-\alpha)\, {}^{t}\tilde{\Sigma} + \alpha\, {}^{t+\Delta t}\tilde{\Sigma}]. \tag{114}$$

Now substituting eqs. (109), (110), (113) and (114) into eq. (102) yields:

$$\begin{aligned} {}^{t+\Delta t}K^{\mathrm{E}}\, U = {} & R + \tilde{B}_L^{\mathrm{T}}\, {}^{t+\Delta t}\tilde{C}^{\mathrm{E}}\tilde{W}\tilde{E}^{TH} + [(1-\alpha)\,\Delta t\, \tilde{B}_L^{\mathrm{T}}\, {}^{t+\Delta t}\tilde{C}^{\mathrm{E}}\tilde{W}\, {}^{t+\alpha\Delta t}\tilde{G}\tilde{D} - \tilde{B}_L^{\mathrm{T}}\, \tilde{C}^{\mathrm{E}}\, {}^{t}\tilde{F}^{\mathrm{E}}\tilde{W}]\, {}^{t}\tilde{\Sigma} \\ & + \alpha\Delta t\, \tilde{B}_L^{\mathrm{T}}\, {}^{t+\Delta t}\tilde{C}^{\mathrm{E}}\, \tilde{W}\, {}^{t+\alpha\Delta t}\tilde{G}\, \tilde{D}\, {}^{t+\Delta t}\tilde{\Sigma}, \end{aligned} \tag{115}$$

where

$${}^{t+\alpha\Delta t}\tilde{G} = {}^{t+\alpha\Delta t}\tilde{\gamma} + {}^{t+\alpha\Delta t}\tilde{\Lambda}. \tag{116}$$

Substituting eqs. (111) and (112) into eq. (98) and then generalizing to a complete set of integration point equations yields:

$$[\tilde{I} + \alpha\Delta t\, {}^{t+\alpha\Delta t}\tilde{G}\, {}^{t+\Delta t}\tilde{C}^{E}\tilde{D}]\, {}^{t+\Delta t}\tilde{\Sigma} = {}^{t+\Delta t}\tilde{C}^{E}(\tilde{B}_L U - \tilde{E}^{TH}) + [\tilde{I} + \tilde{C}^{E}\, {}^{t}\tilde{F}^{E} - (1-\alpha)\,\Delta t\, {}^{t+\alpha t}\tilde{G}\, {}^{t+\Delta t}\tilde{C}^{E}\tilde{D}]\, {}^{t}\tilde{\Sigma}, \tag{117}$$

where $\tilde{I}$ is a $6M \times 6M$ identity matrix. The final set of integration point stress equations is now obtained by substituting eq. (115) and the identity [20]

$$({}^{t+\Delta t}\tilde{C}^{E}\tilde{B}_L\, {}^{t+\Delta t}K^{E^{-1}}\tilde{B}_L^{T} - \tilde{W}^{-1})\,\tilde{W}\tilde{C}^{E}\, {}^{t}\tilde{F}^{E} = -({}^{t+\Delta t}\tilde{C}^{E}\tilde{B}_L\, {}^{t+\Delta t}K^{E^{-1}}\tilde{B}_L^{T}\, {}^{t+\Delta t}\tilde{C}^{E} - {}^{t+\Delta t}\tilde{C}^{E}\tilde{W}^{-1})\,\tilde{W}\tilde{F}^{E} \tag{118}$$

into eq. (119). The result is:

$$\begin{aligned}[\tilde{I} - \alpha\Delta t[{}^{t+\Delta t}\tilde{C}^{E}\tilde{B}_L\, {}^{t+\Delta t}K^{E^{-1}}\tilde{B}_L^{T}\, {}^{t+\Delta t}C^{E} - {}^{t+\Delta t}\tilde{C}^{E}\tilde{W}^{-1}]\,\tilde{W}\, {}^{t+\alpha\Delta t}\tilde{G}\tilde{D}]\, {}^{t+\Delta t}\tilde{\Sigma} = \\ {}^{t+\Delta t}\tilde{C}^{E}\tilde{B}_L\, {}^{t+\Delta t}K^{E^{-1}}R + [{}^{t+\Delta t}\tilde{C}^{E}\tilde{B}_L\, {}^{t+\Delta t}K^{E^{-1}}\tilde{B}_L^{T}\, {}^{t+\Delta t}\tilde{C}^{E} - {}^{t+\Delta t}\tilde{C}\tilde{W}^{-1}]\,\tilde{W}\tilde{E}^{TH} \\ + [\tilde{I} + (1+\alpha)\Delta t[{}^{t+\Delta t}\tilde{C}^{E}\tilde{B}_L\, {}^{t+\Delta t}K^{E^{-1}}\tilde{B}_L^{T}\, {}^{t+\Delta t}\tilde{C}^{E} - {}^{t+\Delta t}\tilde{C}^{E}\tilde{W}^{-1}]\, {}^{t+\alpha\Delta t}\tilde{G}\tilde{D} \\ + [{}^{t+\Delta t}\tilde{C}^{E}\tilde{B}_L\, {}^{t+\Delta t}K^{E^{-1}}\tilde{B}_L^{T}\, {}^{t+\Delta t}\tilde{C}^{E} - {}^{t+\Delta t}\tilde{C}^{E}\tilde{W}^{-1}]\,\tilde{W}\tilde{F}^{E}]\, {}^{t}\tilde{\Sigma}.\end{aligned} \tag{119}$$

We note that eq. (119) shows the contributions to ${}^{t+\Delta t}\tilde{\Sigma}$ from external loading, thermal strains, change in elastic moduli, creep, and plasticity.

To determine if the solution procedure can be made unconditionally stable as discussed in section 3.3, we compare eqs. (39) and (119). It is observed that

$${}^{t+\Delta t}A = {}^{t+\Delta t}\tilde{C}^{E}\tilde{B}_L\, {}^{t+\Delta t}K^{E^{-1}}\tilde{B}_L^{T}\, {}^{t+\Delta t}\tilde{C}^{E} - {}^{t+\Delta t}\tilde{C}^{E}\tilde{W}^{-1}, \tag{120}$$

$${}^{t+\alpha\Delta t}C = \tilde{W}\, {}^{t+\alpha\Delta t}\tilde{G}\tilde{D} \tag{121}$$

and

$$\begin{aligned} S &= \tilde{W}\tilde{F}^{E}, \\ L &= {}^{t+\Delta t}\tilde{C}^{E}\tilde{B}_L\, {}^{t+\Delta t}K^{E^{-1}}R, \\ T &= \tilde{W}\tilde{E}^{TH}. \end{aligned} \tag{122}$$

The matrices S, L, and T satisfy their basic definitions accompanying eq. (39) and ${}^{t+\Delta t}A$ and ${}^{t+\alpha\Delta t}C$ are symmetric. However, since the criteria for unconditional stability also assume that ${}^{t+\Delta t}A$ is negative definite and ${}^{t+\alpha\Delta t}C$ is positive semi-definite, the properties of these matrices must be investigated.

The matrix ${}^{t+\Delta t}A$ is examined in Appendix A. It is shown therein that the matrix is negative definite only when the elastic stiffness matrix ${}^{t+\Delta t}K^{E}$ is approximate. In the case of ${}^{t+\alpha\Delta t}C$, the structure of the matrix is:

$${}^{t+\alpha\Delta t}C = \begin{bmatrix} w_1({}^{t+\alpha\Delta t}\gamma_1 + {}^{t+\alpha\Delta t}\Lambda_1)D & & \\ & w_2({}^{t+\alpha\Delta t}\gamma_2 + {}^{t+\alpha\Delta t}\Lambda_2)D & \\ & & \ddots \\ & & w_M({}^{t+\alpha\Delta t}\gamma_M + {}^{t+\alpha\Delta t}\Lambda_M)D \end{bmatrix} \tag{123}$$

The terms ${}^{t+\alpha\Delta t}\gamma_i$ and ${}^{t+\alpha\Delta t}\Lambda_i$ are > 0, the Gauss weights w_j are > 0, and D is positive semi-definite. Therefore, each submatrix in ${}^{t+\alpha\Delta t}C$ is positive semi-definite and so is the complete matrix.

Thus, unconditional stability is obtained when $\alpha \geq \frac{1}{2}$ and the elastic stiffness matrix is approximate.

3.4. General case

In this section we present an algorithm for the general case in which one time step size is used for the nodal point displacements and a smaller one for the integration point stresses, plastic strains, and creep strains [16–19]. We assume that a numerical solution has been obtained at discrete time points $\Delta t, 2\Delta t, \ldots, t$ and the solution at time $t + \Delta t$ is desired.

3.4.1. Equilibrium and constitutive equations

The virtual work equation and the thermo-elastic-plastic and creep constitutive equations have been presented in eqs. (60)–(64). In addition, eqs. (66) and (67) remain directly applicable.

3.4.2. Algorithm development

The time step Δt is divided into q, not necessarily equal, subdivisions $\delta\tau$ with the time at the start and end of the jth subdivision denoted by τ_j and τ_{j+1}, respectively. At the end of the jth subdivision, the stresses are given by

$$ {}^{\tau_{j+1}}\boldsymbol{\sigma} = {}^{\tau_{j+1}}\boldsymbol{C}^{\mathrm{E}}({}^{\tau_{j+1}}\boldsymbol{e} - {}^{\tau_{j+1}}\boldsymbol{e}^{\mathrm{P}} - {}^{\tau_{j+1}}\boldsymbol{e}^{\mathrm{C}} - {}^{\tau_{j+1}}\boldsymbol{e}^{\mathrm{TH}}) , \tag{124} $$

where ${}^{\tau_{j+1}}\boldsymbol{e}^{\mathrm{P}}$ and ${}^{\tau_{j+1}}\boldsymbol{e}^{\mathrm{C}}$ are evaluated using the α-method. This evaluation is accomplished using eqs. (68)–(73) so as to obtain the decompositions

$$ {}^{\tau_{j+1}}\boldsymbol{e}^{\mathrm{P}} = {}^{\tau_j}\boldsymbol{e}^{\mathrm{P}} + \boldsymbol{e}^{\mathrm{P}} , \tag{125} $$

$$ {}^{\tau_{j+1}}\boldsymbol{e}^{\mathrm{C}} = {}^{\tau_j}\boldsymbol{e}^{\mathrm{C}} + \boldsymbol{e}^{\mathrm{C}} \tag{126} $$

and then the increments

$$ \boldsymbol{e}^{\mathrm{P}} = \delta\tau\, {}^{\tau_j+\alpha\delta\tau}\dot{\boldsymbol{e}}^{\mathrm{P}} = \delta\tau\, {}^{\tau_j+\alpha\delta\tau}\Lambda\, \boldsymbol{D}\, {}^{\tau_j+\alpha\delta\tau}\boldsymbol{\sigma} , \tag{127} $$

$$ \boldsymbol{e}^{\mathrm{C}} = \delta\tau\, {}^{\tau_j+\alpha\delta\tau}\dot{\boldsymbol{e}}^{\mathrm{C}} = \delta\tau\, {}^{\tau_j+\alpha\delta\tau}\gamma\boldsymbol{D}\, {}^{\tau_j+\alpha\delta\tau}\boldsymbol{\sigma} , \tag{128} $$

where

$$ {}^{\tau_j+\alpha\delta\tau}\boldsymbol{\sigma} = (1-\alpha)\, {}^{\tau}\boldsymbol{\sigma} + \alpha\, {}^{\tau_{j+1}}\boldsymbol{\sigma} \tag{129} $$

and

$$ {}^{\tau_j+\alpha\delta\tau}\Lambda = {}^{\tau_j+\alpha\delta\tau}\Lambda({}^{\tau_j+\alpha\delta\tau}\boldsymbol{\sigma}, {}^{\tau_j+\alpha\delta\tau}\dot{\boldsymbol{e}}, {}^{\tau_j+\alpha\delta\tau}\dot{\boldsymbol{e}}^{\mathrm{C}}, {}^{\tau_j+\alpha\delta\tau}\dot{\theta}, \ldots) ,$$

$$ {}^{\tau_j+\alpha\delta\tau}\gamma = {}^{\tau_j+\alpha\delta\tau}\gamma({}^{\tau_j+\alpha\delta\tau}\boldsymbol{\sigma}, {}^{\tau_j+\alpha\delta\tau}\bar{e}^{\mathrm{H}}, {}^{\tau_j+\alpha\delta\tau}\theta) . \tag{130} $$

Eqs. (124)–(130) are a coupled set of nonlinear, algebraic equations which must be solved for each subdivision at every integration point. After q subdivisions,

$$ \begin{aligned} {}^{t+\Delta t}\boldsymbol{\sigma} &= {}^{\tau_{q+1}}\boldsymbol{\sigma} , \\ {}^{t+\Delta t}\boldsymbol{e}^{\mathrm{P}} &= {}^{\tau_{q+1}}\boldsymbol{e}^{\mathrm{P}} , \\ {}^{t+\Delta t}\boldsymbol{e}^{\mathrm{C}} &= {}^{\tau_{q+1}}\boldsymbol{e}^{\mathrm{C}} . \end{aligned} \tag{131} $$

In addition to the above equations, it is also necessary to relate ${}^{\tau_{j+1}}\boldsymbol{e}$ to ${}^{t+\Delta t}\boldsymbol{e}$, which is obtained using eqs. (65) and (66). Assuming that the nodal point displacements vary linearly with time from t and $t + \Delta t$, we then have

$$ {}^{\tau_{j+1}}\boldsymbol{e} = {}^{t}\boldsymbol{e} + \frac{{}^{t+\Delta t}\boldsymbol{e} - {}^{t}\boldsymbol{e}}{\Delta t}\,(\tau_{j+1} - t) \tag{132} $$

Thus, eq. (66) must be solved simultaneously with the subdivision equations, eqs. (124)–(130). As previously discussed in section 3.3.2, an iterative solution procedure is required. Following the developments in that section, the final algorithm proposed for practical analysis is summarized in table 1. In this table, the right subscript k is

Table 1
Algorithm for practical analysis [a]

(1) Loop to (11) for each solution step.
(2) Set the displacement loop iteration counter $i = 0$ (${}^{t+\Delta t}U^{(0)} = {}^{t}U$, ${}^{t+\Delta t}e^{(0)} = {}^{t}e$).
(3) Loop to (9) for each integration point.
(4) Set the subdivision counter $j = 1$.
(5) Calculate the size $\delta\tau$ of the jth subdivision. When $i = 0$ and $j = 1$, set $\delta\tau = \Delta t$.
(6) Calculate the total strain at the end of the jth subdivision.

$$ {}^{\tau_{j+1}}e^{(i)} = {}^{t}e + \frac{{}^{t+\Delta t}e^{(i)} - {}^{t}e}{\Delta t}\,(\tau_{j+1} - t)\,. \tag{133} $$

(7) Set the integration point loop iteration counter $k = 0$. This indicates conditions at time τ_j.
(8) Solve for ${}^{\tau_{j+1}}e^{\mathrm{P}(i)}_{(k+1)}$, ${}^{\tau_{j+1}}e^{\mathrm{C}(i)}_{(k+1)}$, and ${}^{\tau_{j+1}}\boldsymbol{\sigma}^{(i)}_{(k+1)}$ with ${}^{\tau_{j+1}}e^{(i)}$ held constant.

$$ {}^{\tau_{j+1}}e^{\mathrm{P}(i)}_{(k+1)} = {}^{\tau_j}e^{\mathrm{P}(i)} + \delta t\,{}^{\tau_j+\alpha\delta\tau}\Lambda_{(k)}\,D\,{}^{\tau_j+\alpha\delta\tau}\boldsymbol{\sigma}^{(i)}_{(k)}, $$

$$ \left[I + \alpha\delta\tau\,{}^{\tau_{j+1}}C^{\mathrm{E}}\left[D\,{}^{\tau_j+\alpha\delta\tau}\boldsymbol{\sigma}^{(i)}\frac{\partial\,{}^{\tau_j+\alpha\delta\tau}\gamma^{(i)}}{\partial\,{}^{\tau_j+\alpha\delta\tau}\boldsymbol{\sigma}^{(i)}} + {}^{\tau_j+\alpha\delta\tau}\gamma^{(i)}D\right]_{(k)}\right]{}^{\tau_{j+1}}\boldsymbol{\sigma}^{(i)}_{(k+1)} \tag{134} $$

$$ = {}^{\tau_{j+1}}C^{\mathrm{E}}({}^{\tau_{j+1}}e^{(i)} - {}^{\tau_{j+1}}e^{\mathrm{P}(i)}_{(k+1)} - {}^{\tau_j}e^{\mathrm{C}(i)} - {}^{\tau_{j+1}}e^{\mathrm{TH}} - \partial\tau\,{}^{\tau_j+\alpha\delta\tau}\gamma^{(i)}_{(k)}\,D\,{}^{\tau_j+\alpha\delta\tau}\boldsymbol{\sigma}^{(i)}_{(k)}) $$

$$ + \alpha\delta\tau\,{}^{\tau_{j+1}}C^{\mathrm{E}}\left[D\,{}^{\tau_j+\alpha\delta\tau}\boldsymbol{\sigma}^{(i)}\frac{\partial\,{}^{\tau_j+\alpha\delta\tau}\gamma^{(i)}}{\partial\,{}^{\tau_j+\alpha\delta\tau}\boldsymbol{\sigma}^{(i)}} + {}^{\tau_j+\alpha\delta\tau}\gamma^{(i)}D\right]_{(k)}{}^{\tau_{j+1}}\boldsymbol{\sigma}^{(i)}_{(k)}\,, \tag{135} $$

$$ {}^{\tau_j+\delta\tau}e^{\mathrm{C}(i)}_{(k+1)} = {}^{\tau_j}e^{\mathrm{C}(i)} + \delta\tau\,{}^{\tau_j+\alpha\delta\tau}\gamma^{(i)}_{(k)}D\,{}^{\tau_j+\alpha\delta\tau}\boldsymbol{\sigma}^{(i)}_{(k)} + \alpha\delta\tau\left[D\,{}^{\tau_j+\alpha\delta\tau}\boldsymbol{\sigma}^{(i)}\frac{\partial\,{}^{\tau_j+\alpha\delta\tau}\gamma^{(i)}}{\partial\,{}^{\tau_j+\alpha\delta\tau}\boldsymbol{\sigma}^{(i)}} + {}^{\tau_j+\alpha\delta\tau}\gamma^{(i)}D\right]_{(k)} $$

$$ \times\,({}^{\tau_j+\alpha\delta\tau}\boldsymbol{\sigma}^{(i)}_{(k+1)} - {}^{\tau_j+\alpha\delta\tau}\boldsymbol{\sigma}^{(i)}_{(k)})\,. \tag{136} $$

(9) Check for integration point loop convergence. If $i = 0$, bypass check and go to (3) for the next integration point.

No convergence: $k = k + 1$, go to (8).

Convergence: ${}^{\tau_{j+1}} = t + \Delta t$? ↗ Yes: go to (3) for the next integration point.
↘ No: $j = j + 1$, go to (5) for the next subdivision.

(10) Solve for $\Delta U^{(i+1)}$ and ${}^{t+\Delta t}U^{(i+1)}$ after looping through steps (3)–(9) for each integration point.

$$ {}^{t+\Delta t}K^{\mathrm{E}}\,\Delta U^{(i+1)} = {}^{t+\Delta t}R - \int_V B_L^{\mathrm{T}}\,{}^{t+\Delta t}\boldsymbol{\sigma}^{(i)}\,\mathrm{d}v\,, \tag{137} $$

$$ {}^{t+\Delta t}U^{(i+1)} = {}^{t+\Delta t}U^{(i)} + \Delta U^{(i+1)}\,. \tag{138} $$

(11) Check for displacement loop convergence.

No convergence: $i = i + 1$, go to (3).
Convergence: go to (1) for the next solution step.

[a] Step (1)–(11) is called Displacement Loop and step (3)–(9) is called Integration Point Loop.

the integration point loop iteration counter and the right superscript i is the displacement loop iteration counter.

We note that when there are no creep effects, the scheme is essentially successive substitution. Additionally, the comments given in section 3.3.2 concerning improvement of the displacement loop rate-of-convergence remain relevant. The algorithm presented in table 1 contains as a special case, the algorithm developed and analyzed in section 3.3. That is, when $q = 1$ the general algorithm reduces to the special case.

3.4.3. Stability analysis

We have not yet been able to derive a set of clear and useful equations which relate the entire set of integration point stresses at times Δt and $t + \Delta t$, as was done in the stability analysis described in section 3.3.3. However, by following an approach similar to the one in that section, the integration point computations in eqs. (124)–(130) can be shown to be unconditionally stable for each subdivision when $\alpha \geqslant \frac{1}{2}$ [20]. We therefore infer that the overall solution procedure is also unconditionally stable when $\alpha \geqslant \frac{1}{2}$.

4. Test problems

The material model and solution procedure presented in sections 2 and 3 have been implemented in the finite element computer program ADINA [21], and further details of the implementation are given in [20]. Below we report the numerical solutions obtained for three problems – the creep bending of a cantilever beam, the creep of a pressurized, thick-walled cylinder, and the thermo-elastic-plastic response of a pressurized, thick-walled cylinder. These results indicate some of the actual stability and accuracy characteristics of the solution procedure.

4.1. Creep bending of a cantilever beam

A cantilever beam was subjected to a constant tip bending moment of 6000 in-lbs. The finite element model of the beam is shown in fig. 3. It was possible to model only the portion of the beam above the neutral axis by applying the appropriate displacement boundary conditions to the nodes on the neutral axis. Eight, plane stress, isoparametric elements were used in the model and the element stiffness matrices were evaluated using 3 × 3 Gauss integration. The work-equivalent nodal forces used to represent the tip bending moment were derived from the elastic beam theory stress distribution.

An analytical solution for the transient bending stress distribution was not found. It is possible, however, to obtain an expression for steady state conditions [25] when the uniaxial creep strain rate is of the form

$$ {}^{\tau}\dot{e}^{C} = K\,{}^{\tau}\sigma^{m} , \tag{139}$$

where m and K are constants. The Y-direction bending stress at steady state is then

$$ \sigma_{yy} = -\frac{M}{2b}\frac{2m+1}{m}\left(\frac{h}{2}\right)^{-(2m+1)/m} Z^{1/m} , \quad Z \geqslant 0 , \tag{140}$$

where M, b, h, and Z are defined in fig. 3.

By varying the integration parameter, α, the time step size, Δt, and the number of subdivisions per time step, q, results were obtained for a number of problem cases which are summarized in table 2. Figs. 4–12 present the results for the Y-direction bending stress at the point marked A in fig. 3. Problem cases 1 and 2, which are shown in fig. 4, define a 'baseline solution' against which all of the other results are compared. Since these two cases have a maximum difference between them of approximately 4%, problem case 1 is used in figs. 5 to 12 for the baseline solution.

When $\alpha = 0.0$, $q = 1$, the solution becomes unstable with increasing Δt. On the other hand, stable results are obtained when $q = 10$. This indicates that subdividing the time step (i.e. $q > 1$) can stabilize what would otherwise be an unstable solution.

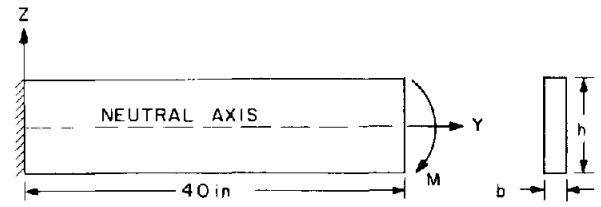

SIDE AND END VIEWS

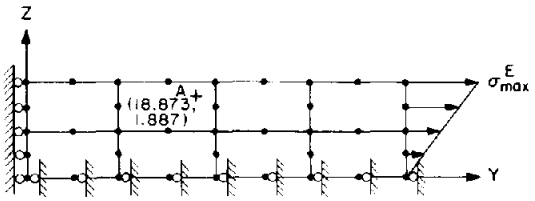

PLANE STRESS MESH

$E = 30 \times 10^6$ psi
$\nu = 0.3$
$\tau_{\bar{e}}^C = K\,\tau_{\bar{\sigma}}^m$
$K = 6.4 \times 10^{-18}$
$m = 3.15$
$b = .3$ in
$h = 4$ in
$M = 6000$ in-lb
$\sigma^E_{max} = 7500$ psi

Fig. 3. Finite element mesh for a cantilever beam.

Table 2
Problem cases for the creep bending of a cantilever beam

Case no.	Integration parameter (α)	Time step size (Δt)	Number of subdivisions per time step [a] (q)
1	0.0	10.0	1
2	0.0	10.0	10
3	0.0	25.0	1
4	0.0	25.0	10
5	0.0	50.0	1
6	0.0	50.0	10
7	0.5	50.0	1
8	0.5	50.0	10
9	0.5	100.0	1
10	0.5	100.0	10
11	0.5	500.0	1
12	0.5	500.0	10
13	1.0	50.0	1
14	1.0	50.0	10
15	1.0	100.0	1
16	1.0	100.0	10
17	1.0	500.0	1
18	1.0	500.0	10

[a] Time step subdivisions are of equal size.

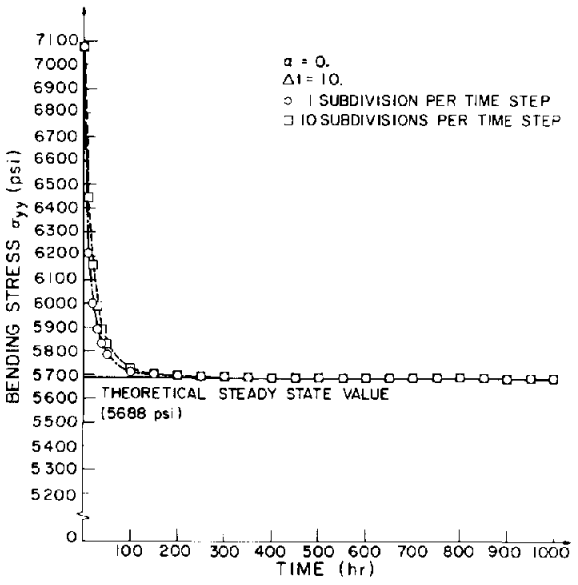

Fig. 4. Baseline solution for the bending stress at location A.

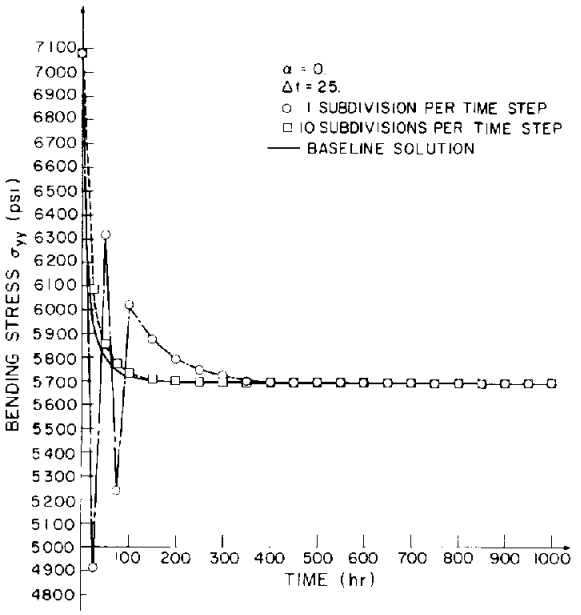

Fig. 5. Bending stress at location A.

For the cases with $\alpha = 0.5, q = 1$ and $\alpha = 1.0, q = 1$, it is possible to obtain stable solutions for values of Δt that are unstable when $\alpha = 0.0, q = 1$. However, when $\alpha = 0.5$ the solution converges to the baseline solution in an oscillatory manner. Since the magnitude of the initial oscillations increases with Δt, the accuracy decreases with increas-

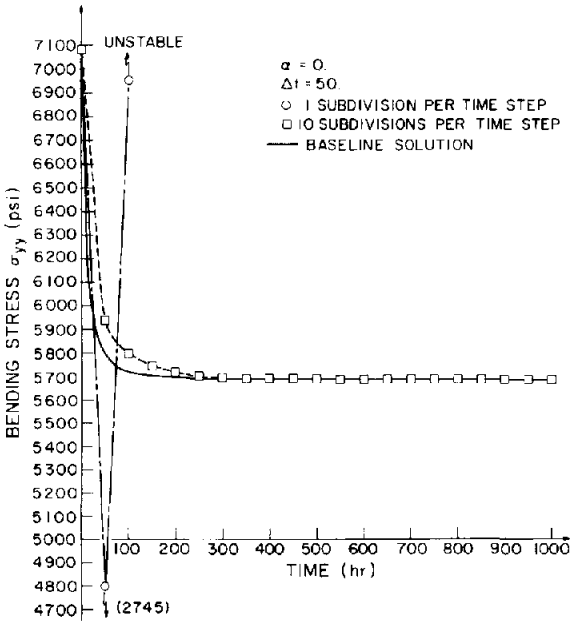

Fig. 6. Bending stress at location A.

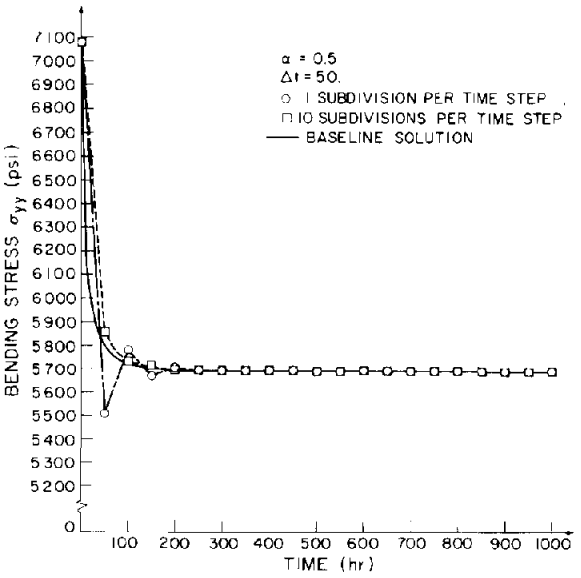

Fig. 7. Bending stress at location A.

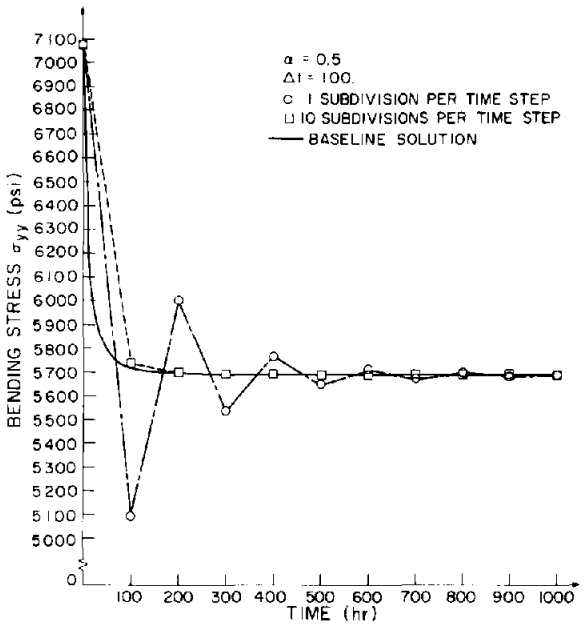

Fig. 8. Bending stress at location A.

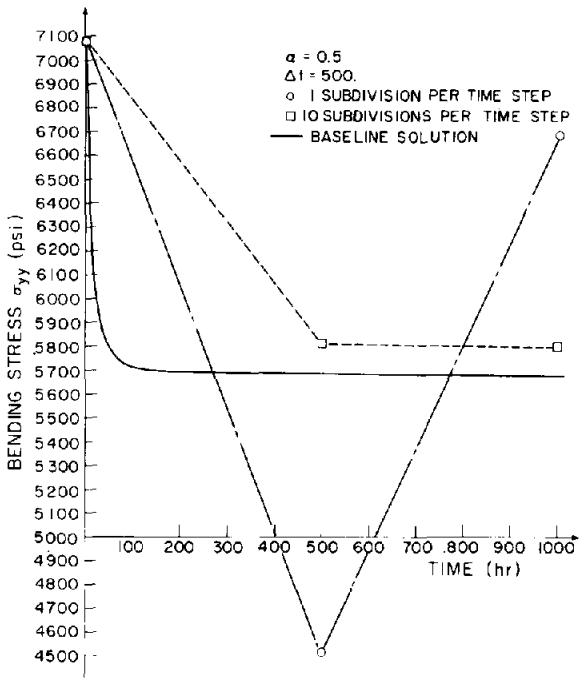

Fig. 9. Bending stress at location A.

ing Δt. For $\alpha = 1.0$, the loss in accuracy with increasing Δt is quite small. If q is increased to 10, the $\alpha = 0.5$ cases no longer exhibit the oscillatory convergence. It is also interesting to note that the $\alpha = 0.5$ cases are slightly more accurate when $\Delta t = 50.0$ and 100.0, but $\alpha = 1.0$ gives better accuracy when $\Delta t = 500$.

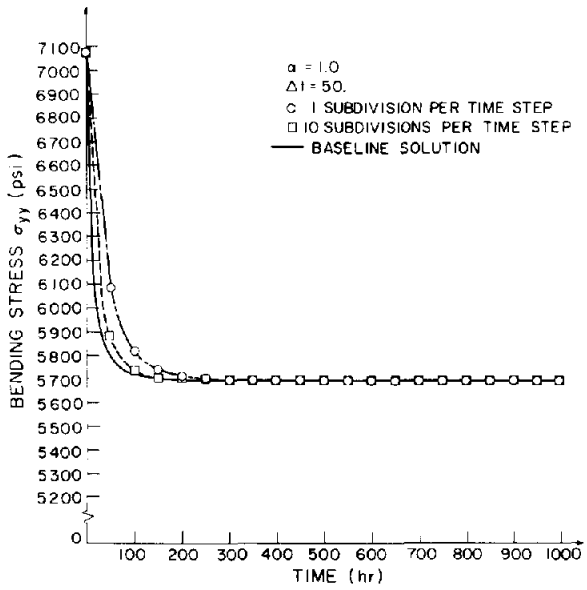

Fig. 10. Bending stress at location A.

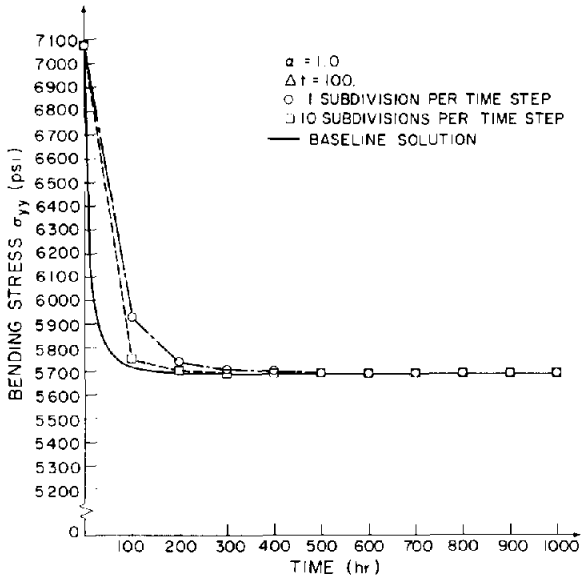

Fig. 11. Bending stress at location A.

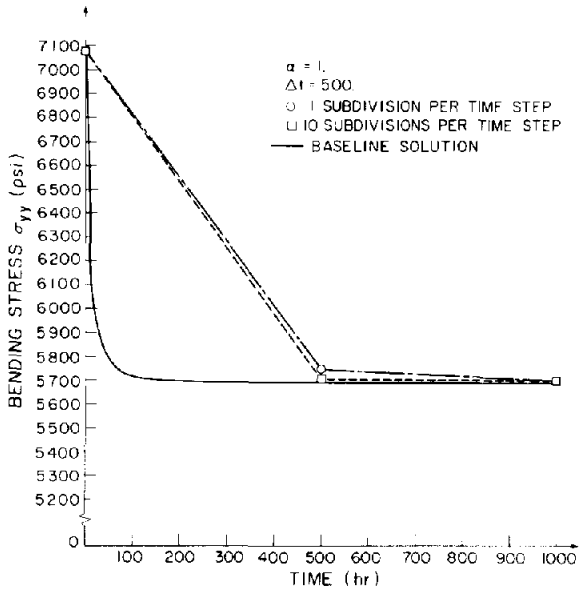

Fig. 12. Bending stress at location A.

4.2. Creep of a thick-walled cylinder

A thick-walled cylinder was subjected to a constant internal pressure of 3650 psi. The finite element model of the cylinder is shown in fig. 13. Plane strain conditions were assumed and twelve axisymmetric elements were used in the model. The element stiffness matrices were evaluated using 3 X 3 Gauss integration. The material

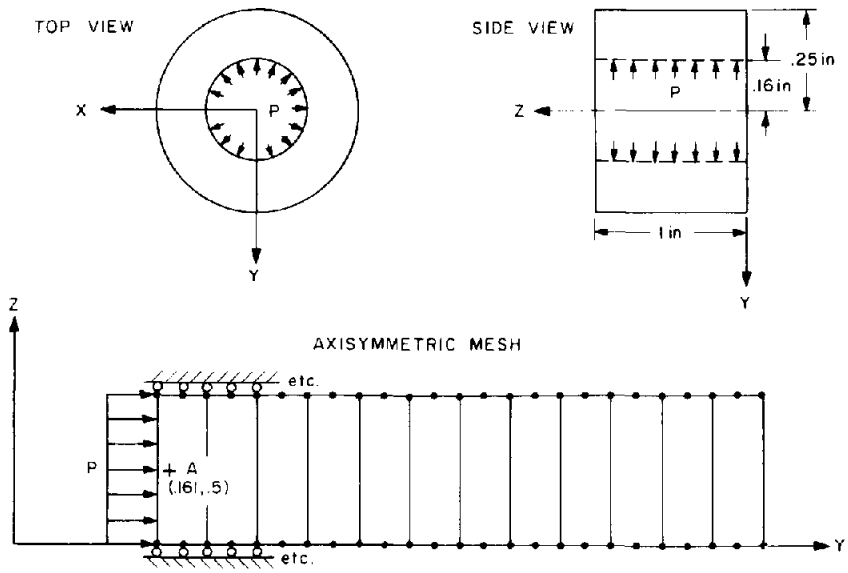

Fig. 13. Finite element mesh for a thick-walled cylinder.

Table 3
Material properties for the thick-walled cylinder

	800°F	900°F	1000°F	1100°F
Young's modulus (psi)	24.07×10^6	23.30×10^6	22.51×10^6	21.71×10^6
Poisson's ratio	0.3	0.3	0.3	0.3
Virgin material yield stress (psi)	1.11×10^4	1.004×10^4	9.344×10^3	9×10^3
Hardening modulus (psi)	7.3×10^5	7.3×10^5	7.3×10^5	7.3×10^5
Mean coefficient of thermal expansion (in/in/°F)	11.18×10^{-6}	11.28×10^{-6}	11.38×10^{-6}	11.48×10^{-6}

All properties were assumed to vary in a piecewise linear manner between the tabulated values.

Uniaxial creep law:

$$\dot{\tau}_e^C = F(1 - e^{-R\tau}) + G\tau,$$
$$F = a_0 \tau_\sigma^{a_1},$$
$$R = a_2 e^{a_3 \tau_\sigma},$$
$$G = a_4[\sinh(a_5 \tau_\sigma)]^{a_6},$$

τ_σ = constant uniaxial stress,

$a_0 = 1.608 \times 10^{-10}$, $a_4 = 6.73 \times 10^{-9}$,
$a_1 = 1.843$, $a_5 = 1.479 \times 10^{-4}$,
$a_2 = 5.929 \times 10^{-5}$, $a_6 = 3.0$.
$a_3 = 2.029 \times 10^{-4}$,

properties at 1100°F and the uniaxial creep law given in table 3 were used. Thermal strains were not considered and there were no plasticity effects.

The cases considered for this problem are summarized in table 4. Figs. 14–19 show the von Mises effective stress (see eq. (3)) at the point marked A in fig. 13. Problem case 1 in fig. 14 is defined to be the 'baseline solution'. When $\alpha = 0.0$, the solution results eventually become unstable as Δt is increased from the baseline value. It is interesting to note that although cases 2 and 3 (figs. 15 and 16) are initially inaccurate, the baseline solution is attained as time increases. When $\alpha = 0.5$ and 1.0, the solution results are stable for $\Delta t = 5000.0$, which is significantly larger than the values possible with $\alpha = 0.0$. However, both solutions initially oscillate about the baseline solution, and although $\alpha = 1.0$ has smaller oscillations, the $\alpha = 0.5$ case attains the baseline solution at an earlier time.

Table 4
Problem cases for the creep of a thick-walled cylinder

Case No.	Integration parameter (α)	Time step size (Δt)	Number of subdivisions per time step (q)
1	0.0	10.0 ($0.0 \leqslant t \leqslant 100.0$) 100.0 ($t > 100.0$)	1
2	0.0	100.0	1
3	0.0	200.0	1
4	0.0	500.0	1
5	0.5	5000.0	1
6	1.0	5000.0	1

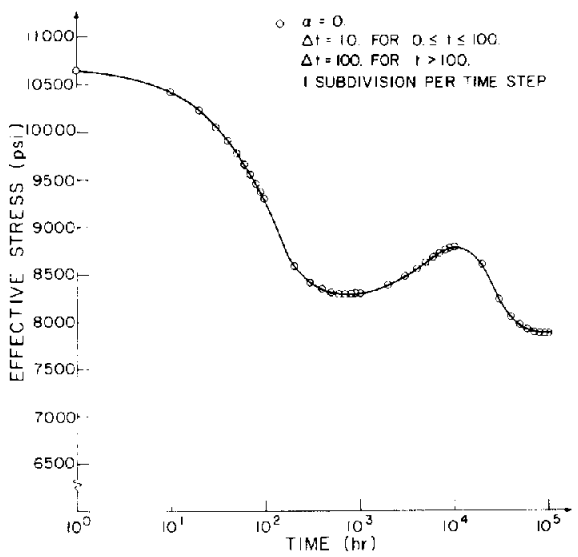

Fig. 14. Baseline solution for the effective stress at location A.

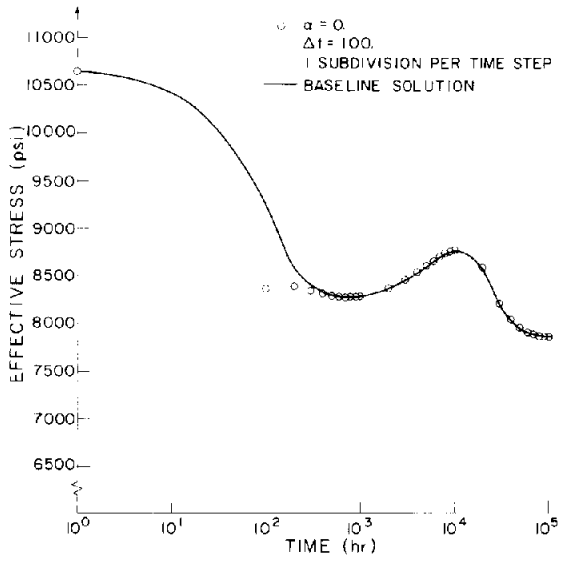

Fig. 15. Effective stress at location A.

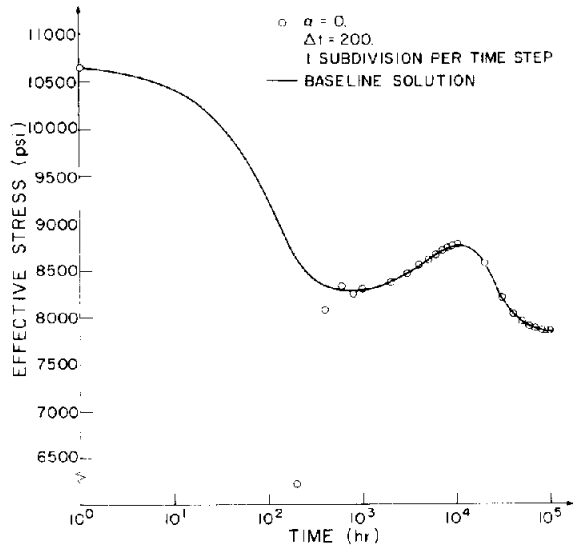

Fig. 16. Effective stress at location A.

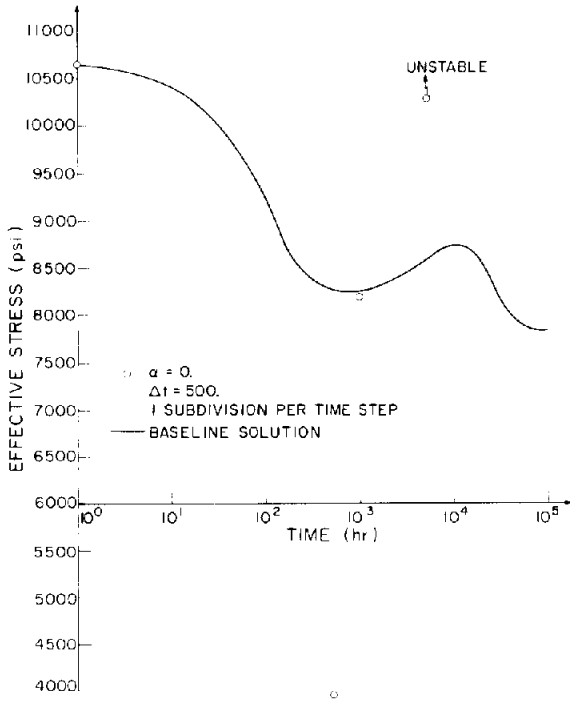

Fig. 17. Effective stress at location A.

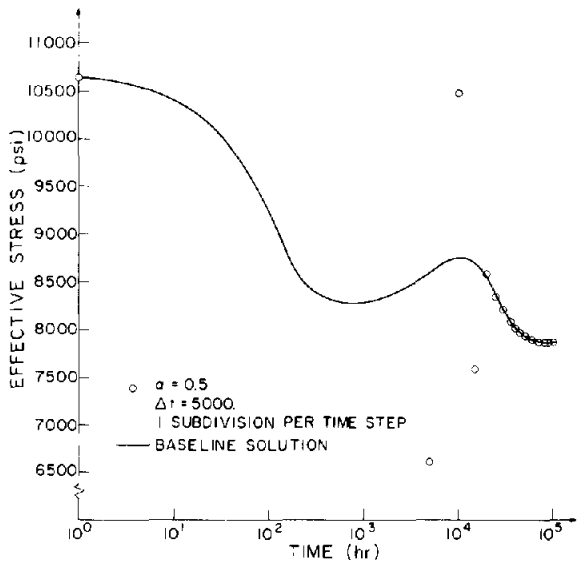

Fig. 18. Effective stress at location A.

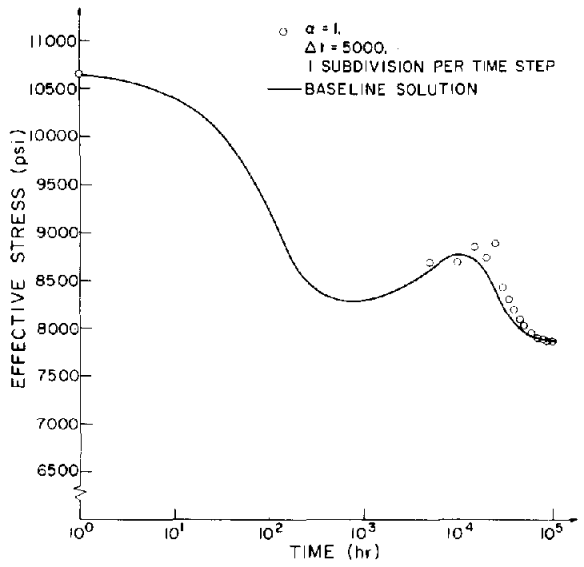

Fig. 19. Effective stress at location A.

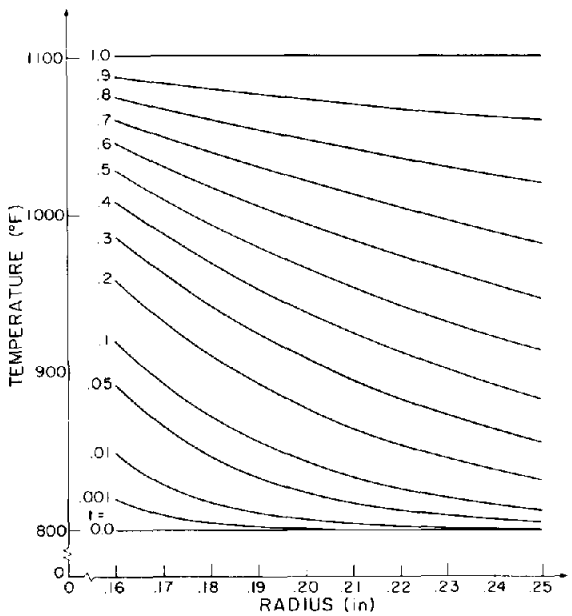

Fig. 20. Radial temperature profiles for the thick-walled cylinder.

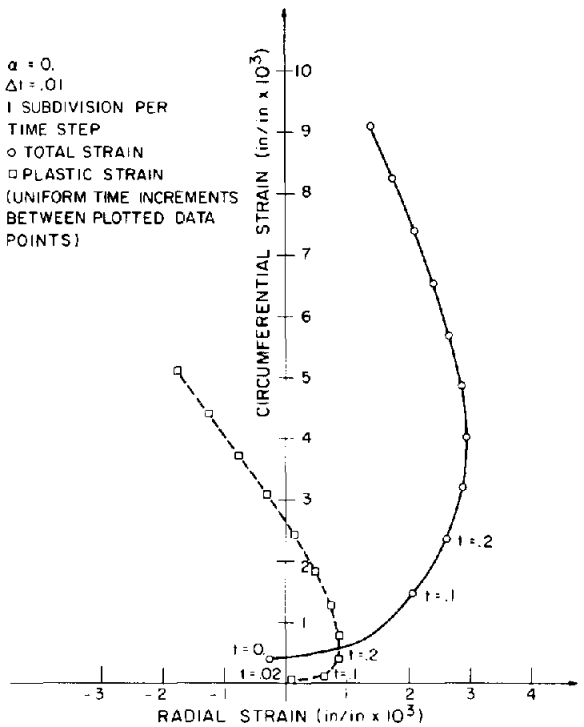

Fig. 21. Baseline solution for the radial and circumferential strains at location A.

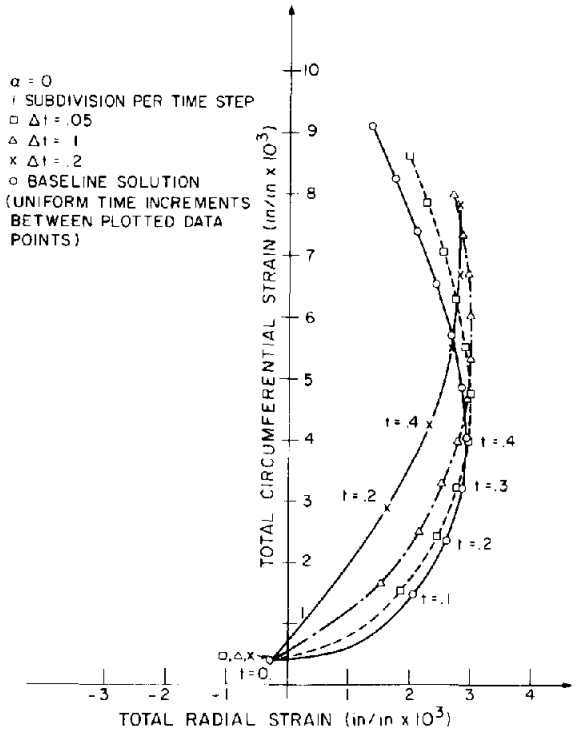

Fig. 22. Total radial and circumferential strains at location A.

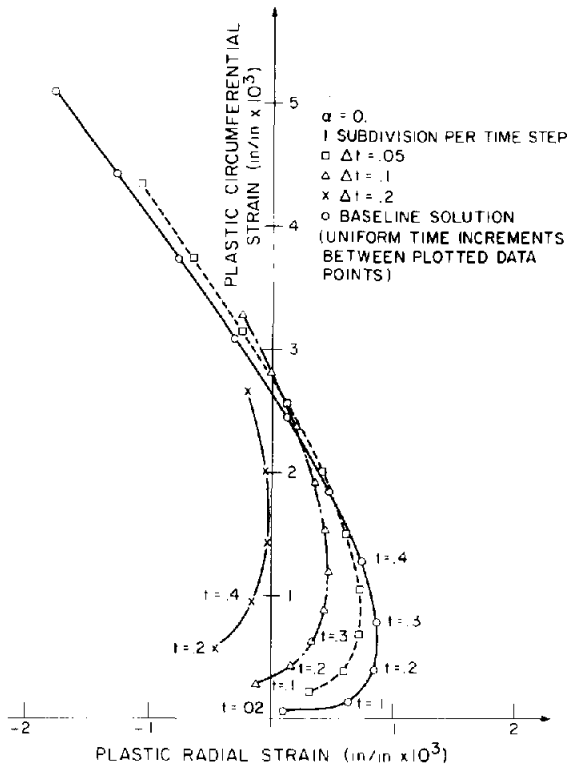

Fig. 23. Plastic radial and circumferential strains at location A.

4.3. Thermo-elastic plastic response of a thick-walled cylinder

A thick walled cylinder was subjected to a constant internal pressure of 3650 psi and a transient temperature distribution. The model of the cylinder is shown in fig. 13 and the temperature dependent material properties are contained in table 3. Kinematic hardening was used and no creep effects were considered. The cylinder was at

Table 5
Problem cases for the thermo-elastic-plastic response of a thick-walled cylinder

Case no.	Integration parameter (α)	Time step size (Δt)	Number of subdivisions per time step [a] (q)
1	0.0	0.01	1
2	0.0	0.05	1
3	0.0	0.1	1
4	0.0	0.2	1
5	0.0	0.05	5
6	0.0	0.1	10
7	0.0	0.2	20

[a] Time step subdivisions are of equal size.

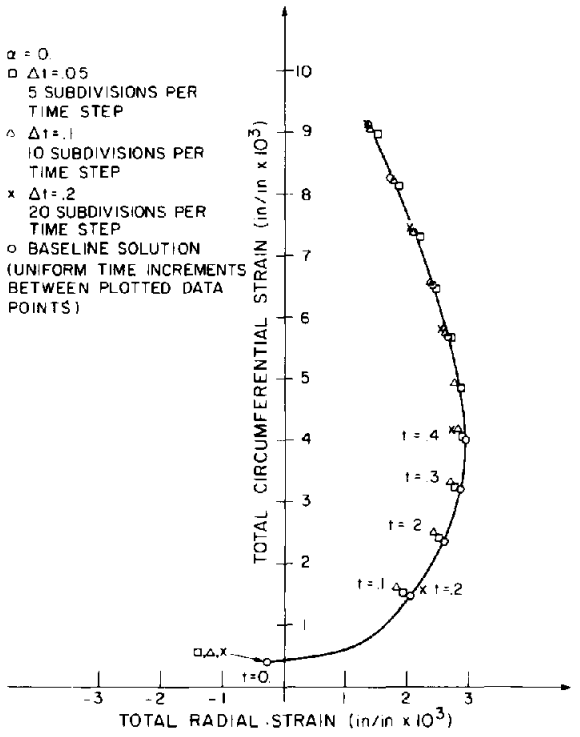

Fig. 24. Total Radial and circumferential strains at location A.

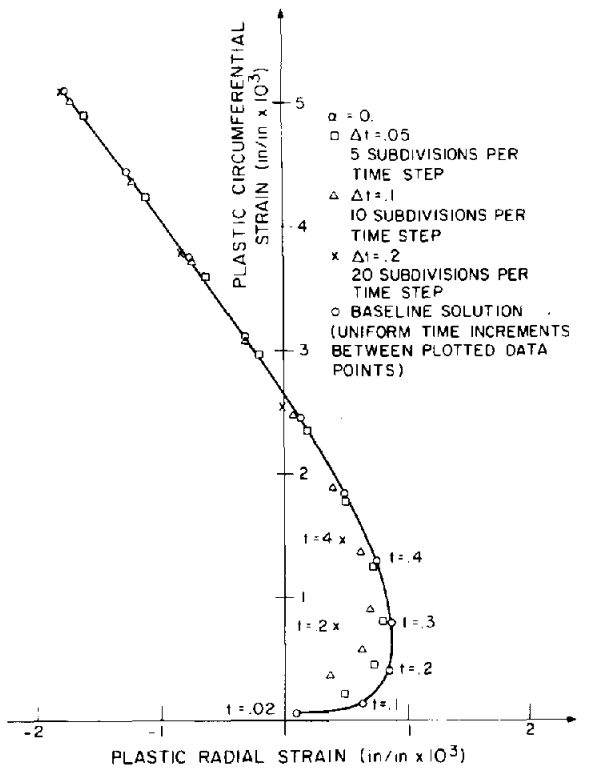

Fig. 25. Plastic radial and circumferential strains at location A.

800°F (reference temperature) at the start of the transient and the radial temperature distribution was of the form

$$^{\tau}\theta = 800 + 300\,\tau^{0.4}\exp\left(\frac{Y-0.16}{0.09}\ln\tau\right), \quad \tau > 0\,. \tag{141}$$

Radial temperature profiles at various times are shown in fig. 20.

The cases considered for this problem are summarized in table 5. Figures 21 to 25 show radial and circumferential strain components (total and plastic) at the point marked A in fig. 13. Problem case 1 in fig. 21 is defined to be the 'baseline solution'. In contrast to the results for the previous two problems, increasing Δt when $\alpha = 0.0$ only causes the solution results to become more inaccurate. The growth of an oscillating instability is not observed. When $q > 1$, a significant improvement in accuracy is obtained for all values of Δt considered.

5. Conclusions

In this paper we have presented an efficient procedure for the finite element solution of problems with thermo-elastic-plastic and creep behavior. We believe that it is an effective tool for engineering analysis.

The material model used in conjunction with the solution procedure is based on the classical theories of plasticity and creep. All assumptions made in the derivation of the material model are clearly stated and the model's range of applicability is discussed. The solution procedure is based on a one-parameter integration scheme and can be made unconditionally stable. The requirements for unconditional stability are obtained from a thorough theo-

retical stability analysis. Numerical results are reported for three test problems. These results show the actual numerical characteristics of the implemented procedure and it is concluded that they agree with the predictions of the theoretical stability analysis.

We plan to obtain additional solutions using the procedure and to report these results at a future date. Since the whole development was carried out with the goal of providing engineers with a means for effectively solving practical thermo-elastic-plastic and creep problems, we are also looking forward to exchanging experiences with other ADINA users.

Acknowledgement

We gratefully acknowledge the financial support of the ADINA users group and the Forschungszentrum GKSS, W. Germany for this research work.

Appendix A. Investigation of the properties of the matrix

$$^{t+\Delta t}A = {}^{t+\Delta t}\tilde{C}^{E}\tilde{B}_L\ {}^{t+\Delta t}K^{E\,-1}\tilde{B}_L^{T}\ {}^{t+\Delta t}\tilde{C}^{E} - {}^{t+\Delta t}\tilde{C}^{E}\tilde{W}^{-1}\,.$$

Instead of dealing directly with $^{t+\Delta t}A$, we examine the expression

$$b = \tilde{x}^{T}\tilde{W}\ {}^{t+\Delta t}A\ \tilde{W}\tilde{x}\,, \tag{A.1}$$

where $\tilde{W}$ is defined in eq. (107) and $\tilde{x}$ is an arbitrary vector. It can be shown [20] that $\tilde{W}\ {}^{t+\Delta t}A\ \tilde{W}$ being negative definite is necessary and sufficient for $^{t+\Delta t}A$ to be so also.

Consider an arbitrary body subjected to surface tractions $^{t+\Delta t}f^{S}$ and body forces $^{t+\Delta t}f^{B}$ which cause an equilibrium elastic stress and strain field

$$^{t+\Delta t}\sigma = {}^{t+\Delta t}C^{E}x\,. \tag{A.2}$$

We assume that we have a finite element representation of the body and interpret $\tilde{x}$ as a supervector of the actual elastic strains at the element integration points. By eq. (103),

$$\begin{aligned}\tilde{x}^{T}\tilde{W}\,{}^{t+\Delta t}\tilde{C}^{E}\tilde{x} &= \int_{v} x^{T}\,{}^{t+\Delta t}C^{E}x\,dv\\ &= 2U_s^{e}\,,\end{aligned} \tag{A.3}$$

where U_s^{e} is the exact elastic strain energy [38,39,44]. In eq. (A.3), we have assumed that a sufficient number of integration points have been used so that the integration is performed exactly. In practice, this assumption is frequently violated and, indeed, it may not be possible to perform an exact integration numerically. Similarly, we find that

$$\tilde{B}_L^{T}\,{}^{t+\Delta t}\tilde{C}^{E}\tilde{W}\tilde{x} = \int_{v} B_L^{T}\,{}^{t+\Delta t}C^{E}x\,dv = \int_{v} B_L^{T}\,{}^{t+\Delta t}\sigma\,dv = \sum_{m=1}^{N}\int_{v^{(m)}} B_L^{T}\,{}^{t+\Delta t}\sigma\,dv\,, \tag{A.4}$$

where N is the number of elements in the finite element assemblage.

Consider the virtual work principle [38–40,44]

$$\int_{v}\delta e^{T}\,{}^{t+\Delta t}\sigma\,dv = \int_{s}\delta u^{T}\,{}^{t+\Delta t}f^{S}\,ds + \int_{v}\delta u^{T}\,{}^{t+\Delta t}f^{B}\,dv\,, \tag{A.5}$$

where δu and δe are arbitrary, kinematically-admissible variations. Once again noting eq. (103), Eq. (A.5) can be written as

$$\sum_{m=1}^{N} \int_{v^{(m)}} \delta e^{\mathrm{T}}\, {}^{t+\Delta t}\sigma \, \mathrm{d}v = \sum_{m=1}^{N} \int_{s^{(m)}} \delta u^{\mathrm{T}}\, {}^{t+\Delta t}f^{\mathrm{S}} \, \mathrm{d}s + \sum_{m=1}^{N} \int_{v^{(m)}} \delta u^{\mathrm{T}}\, {}^{t+\Delta t}f^{\mathrm{B}} \, \mathrm{d}v \,. \tag{A.6}$$

Since ${}^{t+\Delta t}\sigma$ is in equilibrium with the applied loading, eq. (A.6) must hold for all admissible variations. Furthermore, the equation must also hold when the finite element approximations [40,41]

$$\delta u = H\, \delta U \,, \tag{A.7}$$

$$\delta e = B_L \delta U \tag{A.8}$$

are employed. Thus, we obtain

$$\sum_{m=1}^{N} \int_{v^{(m)}} B_L^{\mathrm{T}}\, {}^{t+\Delta t}\sigma \, \mathrm{d}v = \sum_{m=1}^{N} \int_{s^{(m)}} H^{\mathrm{T}}\, {}^{t+\Delta t}f^{\mathrm{S}} \, \mathrm{d}s + \sum_{m=1}^{N} \int_{v^{(m)}} H^{\mathrm{T}}\, {}^{t+\Delta t}f^{\mathrm{B}} \, \mathrm{d}v = {}^{t+\Delta t}R \tag{A.9}$$

where ${}^{t+t}R$ is the work-equivalent, nodal point force vector.

Substituting eqs. (A.3), (A.4) and (A.9) into eq. (A.1) results in

$$b = {}^{t+\Delta t}R^{\mathrm{T}}\, {}^{t+\Delta t}K^{\mathrm{E}^{-1}}\, {}^{t+\Delta t}R - 2U_{\mathrm{s}}^{\mathrm{e}} \,. \tag{A.10}$$

It can be shown for a linear elastic system [40,41] that

$${}^{t+\Delta t}R\, {}^{t+\Delta t}K^{\mathrm{E}^{-1}}\, {}^{t+\Delta t}R = 2U_{\mathrm{s}}^{\mathrm{a}} \,, \tag{A.11}$$

where $U_{\mathrm{s}}^{\mathrm{a}}$ is the elastic strain energy of the finite element approximation. Since $U_{\mathrm{s}}^{\mathrm{a}}$ is a lower bound to the exact elastic strain energy [38–40,44], it follows that $b \leqslant 0$.

When $b \leqslant 0$, the matrix ${}^{t+\Delta t}A$ is negative semi-definite. However, in most applications we find that $U_{\mathrm{s}}^{\mathrm{a}} < U_{\mathrm{s}}^{\mathrm{e}}$, due to the approximate nature of the elastic stiffness matrix. Then ${}^{t+\Delta t}A$ is negative definite.

References

[1] J.H. Argyris, J. Royal Aero. Soc. 69 (1965) 633–635.
[2] J.H. Argyris and D.W. Scharpf, Z. Ang. Math. and Phys. 23 (1972) 517–571.
[3] K.J. Willam, J. Comp. and Struct. 8 (1978) 511–531.
[4] J.H. Argyris, L.E. Vaz and K.J. Willam, Comput. Meths. Appl. Mech. Engrg. 16 (1978) 231–277.
[5] I. Cormeau, Internat. J. Numer. Meth. Engrg. 9 (1975) 109–127.
[6] T.J.R. Hughes and R.L. Taylor, J. Comput. and Struct., 8 (1978) 167–173.
[7] G. Greenbaum and M. Rubinstein, Nucl. Engrg. Des. 7 (1968) 379–397.
[8] O.C. Zienkiewicz, S. Valliappan and I.P. King, Internat. J. Numer. Meth. Engrg. 1 (1969) 75–100.
[9] G.C. Nayak and O.C. Zienkiewicz, Internat. J. Numer. Meth. Engrg, 3 (1972) 113–135.
[10] M.B. Kranchi, O.C. Zienkiewicz and D.R.J. Owen, Internat. J. Numer. Meth. Engrg. 12 (1978) 169–181.
[11] W. Pilkey, K. Saczalski and H. Schaeffer, Structural Mechanics Computer Programs (Univ. Press of Virginia, Charlottesville, VA, 1974).
[12] J.A. Stricklin, W.E. Haisler and W.H. Riesemann, AIAA J. 11, (3) (1973) 292–299,
[13] R. Gallagher, J. Padlog and P.P. Bijlaard, Amer. Rocket Soc. J. (May 1962) 700–707.
[14] P. Sharifi and D.N. Yates, AIAA J. 12 (1973) 1210–1215.
[15] N.A. Cyr and R.D. Teter, J. Comput. and Struct. 3 (1973) 849–863.
[16] K.J. Bathe, H. Ozdemir and E.L. Wilson, Report UCSESM 74-4, Civil Engineering Dept., University of California, Berkeley
[17] K.J. Bathe, Report 82448-2, Acoustics and Vibration Lab., Mechanical Engineering Dept., M.I.T. (May 1976; rev. May 1977).
[18] M.D. Snyder and K.J. Bathe, Report 82448-3, Acoustics and Vibration Lab., Mechanical Engineering Dept., M.I.T. (June 1977).

[19] D. Bushnell, Internat. J. Numer. Meth. Engrg. 11 (1977) 683–708.
[20] M.D. Snyder and K.J. Bathe, Report 82448-10, Acoustics and Vibration Lab., Mechanical Engineering Dept., M.I.T. (December 1980).
[21] K.J. Bathe, Report 82448-1, Acoustics and Vibration Lab., Mechanical Engineering Dept., M.I.T. (September 1975; rev. December 1978).
[22] K.J. Bathe and M.R. Khoshgoftaar, Nucl. Engrg. Des. 51 (1979) 389–401.
[23] T.J.R. Hughes, Comput. Meths. Appl. Mech. Engrg. 10 (1977) 135–141.
[24] K.J. Bathe and A. Cimento, Comput. Mech. Appl. Meth. Engrg. 22 (1980) 59–85.
[25] R.K. Penny and D.L. Marriott, Design for Creep (McGraw-Hill, London, 1971).
[26] I. Finnie and W.R. Heller, Creep of Engineering Materials (McGraw-Hill, New York, 1959).
[27] C.E. Pugh, J.M. Corum, K.C. Liu and W.L. Greenstreet, Report TM-3602, Oak Ridge National Laboratory, Oak Ridge, TN (1972).
[28] C.E. Pugh et al., Report ORNL-5014, Oak Ridge National Laboratory, Oak Ridge, TN (1974).
[29] P.M. Naghdi (Pergamon Press, Oxford 1960) pp. 121–169.
[30] D.C. Drucker, Proc. 1st U.S. Natl. Congress Appl. Mech., 1952, pp. 478–491.
[31] D.C. Drucker, Extension of the stability postulate with emphasis on temperature changes, Proc. 1st Symp. Naval Struc. Mech. (Pergamon Press, Oxford, 1960) pp. 407–455.
[32] D.R. Bland, Proc. 9th Int. Congress Appl. Mech., 1957, pp. 45–50.
[33] W. Prager, J. Appl. Mech. (1970) 728–737.
[34] R.T. Shield and H. Ziegler, Z. Ang. Math. and Phys. IXA (1958) 260–276.
[35] H. Ziegler, Quart. Appl. Math. 17 (1959) 55–65.
[36] T.Y. Chang, ASCE, J. Engrg. Mech. Div. 99 (1973) 423–428.
[37] W. Prager, Proc. Koninklijke Nederlandse Akademie van Wetenschappen 61 (1958) 176–182.
[38] Y.C. Fung, Foundations of Solid Mechanics (Prentice-Hall, Englewood Cliffs, NJ 1976).
[39] L.E. Malvern, Introduction to the Mechanics of a Continuous Medium (Prentice-Hall, Englewood Cliffs, NJ, 1969).
[40] K.J. Bathe and E.L. Wilson, Numerical Methods in Finite Element Analysis (Prentice-Hall, Englewood Cliffs, NJ, 1976).
[41] O.C. Zienkiewicz, The Finite Element Method in Engineering Science (McGraw-Hill, London, 1971).
[42] G. Dahlquist and A. Björck, Numerical Methods (Prentice-Hall, Englewood Cliffs, NJ, 1974).
[43] C.W. Gear, Numerical Initial Value Problems in Ordinary Differential Equations (Prentice-Hall, Englewood Cliffs, NJ 1971).
[44] H.L. Langhaar, Energy Methods in Applied Mechanics (John Wiley, New York, 1962).